A computational model explains and predicts substantia nigra pars reticulata responses to pallidal and striatal inputs

Ryan S. Phillips[1,3], **Ian Rosner**[2,3], **Aryn H. Gittis**[2,3], **Jonathan E. Rubin**[1,3]

***For correspondence:** jonrubin@pitt.edu (JER)

[1]Department of Mathematics, University of Pittsburgh; [2]Department of Biological Sciences, Carnegie Mellon University; [3]Center for the Neural Basis of Cognition, Pittsburgh, PA

Abstract As a rodent basal ganglia (BG) output nucleus, the substantia nigra pars reticulata (SNr) is well positioned to impact behavior. SNr neurons receive GABAergic inputs from the striatum (direct pathway) and globus pallidus (GPe, indirect pathway). Dominant theories of action selection rely on these pathways' inhibitory actions. Yet, experimental results on SNr responses to these inputs are limited and include excitatory effects. Our study combines experimental and computational work to characterize, explain, and make predictions about these pathways. We observe diverse SNr responses to stimulation of SNr-projecting striatal and GPe neurons, including biphasic and excitatory effects, which our modeling shows can be explained by intracellular chloride processing. Our work predicts that ongoing GPe activity could tune the SNr operating mode, including its responses in decision-making scenarios, and GPe output may modulate synchrony and low-frequency oscillations of SNr neurons, which we confirm using optogenetic stimulation of GPe terminals within the SNr.

Introduction

The substantia nigra pars reticulata (SNr) is the primary output nucleus of the rodent basal ganglia (BG) and hence likely plays a key role in the behavioral functions, such as decision-making and action selection, suppression, or tuning, to which the BG contribute. The SNr exhibits intrinsic spiking activity, resulting in ongoing GABAergic outputs to specific thalamic sites, which are believed to suppress unwanted or spurious movements. While the literature on signal transmission through the basal ganglia emphasizes the projection from the subthalamic nucleus to the SNr, the SNr also receives converging $GABA_A$-receptor mediated synaptic inputs associated with the two major transmission channels through the BG, the direct and indirect pathways. Thus, the behavioral influence of the BG is ultimately regulated by how the SNr integrates these inputs.

Although dominant theories of action selection strongly rely on the inhibitory actions of these pathways on SNr, the details of this integration process have not been thoroughly investigated and remain poorly understood. Interestingly, the inputs to SNr from the two pathways feature distinct characteristics. Indirect pathway GABAergic projections to SNr arise from the external segment of the globus pallidus (GPe), which engages in tonic spiking activity; occur via basket-like synapses around the soma of SNr neurons; and exhibit short-term depression. Direct pathway inputs are delivered by striatal (Str) neurons, which spike much more sparsely; are located on distal

dendrites; and exhibit short-term facilitation (***Smith and Bolam, 1991***; ***Von Krosigk et al., 1992***; ***Connelly et al., 2010***; ***Lavian and Korngreen, 2016***). The complexity of how these aspects interact may have hindered the study of the convergence of these inputs to the SNr, yet there may be an additional, easily overlooked factor influencing the process as well: GABA dynamics (***Raimondo et al., 2012***; ***Doyon et al., 2011***, ***2016b***). The ongoing activity of GPe neurons would likely induce a large tonic chloride load on SNr neurons, potentially depolarizing the GABA reversal potential, E_{GABA}. Although striatal inputs are less frequent, their impacts would be affected by chloride accumulation, which could be exaggerated in smaller dendritic compartments, and by associated variability of E_{GABA}. Indeed, past studies have reported E_{GABA} values that vary over a relatively wide range, from -80 to -55 mV, in SNr (***Giorgi et al., 2007***; ***Connelly et al., 2010***; ***Higgs and Wilson, 2016***; ***Simmons et al., 2018***). Moreover, earlier experiments showed excitatory effects along with inhibitory ones from stimulation of SNr-projecting Str neurons *in vivo* (***Freeze et al., 2013***), which could relate to chloride regulation as well.

To study this complex combination of effects and their possible functional consequences, we developed a computational model of an SNr neuron including somatic and dendritic compartments and the corresponding GABAergic inputs as well as the dynamics of intracellular chloride and E_{GABA}. We used this model to investigate the influence of GABAergic synaptic transmission from GPe, Str, and SNr collaterals on SNr activity under behaviorally relevant conditions. We found that with the inclusion of short-term synaptic plasticity tuned to fit previous data, the model's dynamics matched a range of experimental findings on SNr firing patterns, including our own new results from optogenetic stimulation in mice. Given this agreement, we used the model to generate novel predictions about how direct and indirect pathway inputs may shape SNr activity patterns in functional settings involving both pathways. Specifically, we predict that variations in the level of GPe activity could interact with sparse SNr reciprocal interconnectivity to provide an effective mechanism to tune SNr synchrony and the emergence of low-frequency oscillations, and we present experimental data based on optogenetic stimulation of GABAergic GPe terminals in the SNr that provides evidence of this effect. We also predict that ongoing high-frequency GPe activity could serve a modulatory role in action selection by adjusting the effectiveness of lower-frequency direct pathway Str signals at pausing SNr outputs to downstream targets, as would be needed to allow action selection. The convergence of multiple $GABA_A$ receptor-mediated synaptic input streams onto individual neurons, such as pyramidal neurons in cortex, represents a common scenario in neural circuitry, and our results suggest that intracellular Cl^- levels should also be considered in analyzing the integration of GABAergic inputs by neurons in brain regions beyond the SNr.

Results

Conductance-Based SNr Model

Due to the positioning of the SNr within the BG, synaptic integration of GABAergic projections from the direct (Str) and indirect (GPe) pathways in the SNr is likely a critical factor in BG function. Nonetheless, the effects of these two pathways on SNr activity are not well understood. Complicating matters, GPe and Str inputs form synapses on disparate locations on SNr neurons, undergo distinct short-term synaptic plasticity and likely have differing susceptibilities to breakdown of E_{GABA}, mediated by the Cl^- load. Therefore, to investigate synaptic integration of GPe and Str GABAergic inputs to the SNr in more detail, we constructed a conductance-based neuron model with somatic and dendritic compartments (Fig. 1). The two compartments are electrically coupled and intracellular Cl^- concentration ($[Cl^-]_i$) is maintained in each compartment by the potassium-chloride co-transporter (KCC2). The baseline firing rate ($\approx 10Hz$) and properties of the model are tuned to match experimental data (***Richards et al., 1997***; ***Atherton and Bevan, 2005***; ***Yanovsky et al., 2006***; ***Zhou et al., 2008***). For a full model description see Methods.

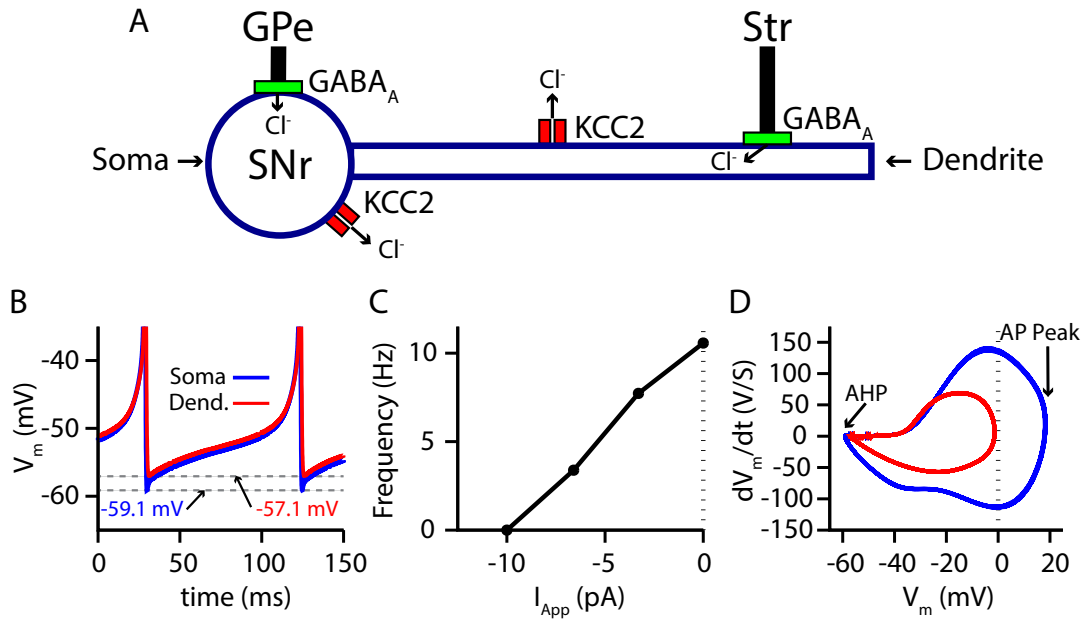

Figure 1. Two-compartment SNr model neuron includes currents that affect $[Cl^-]_i$ and produces appropriate dynamics. (A) Schematic diagram of the model. (B) Tonic spiking voltage traces for both compartments, with minimum voltages labeled. (C) Model f-I curve. (D) Phase plot of the rate of change of the membrane potential (dV_m/dt) against the membrane potential (V_m) showing afterhyperpolarization (AHP) and spike height (AP Peak) for both compartments. The baseline firing rate is tuned to match data from *in vitro* mouse and rat slice recordings (***Richards et al., 1997***; ***Atherton and Bevan, 2005***; ***Yanovsky et al., 2006***; ***Zhou et al., 2008***)

Short-term synaptic depression and facilitation of GPe and Str synaptic projections

The GABAergic synapses from the GPe and Str neurons undergo short-term synaptic depression and facilitation, respectively. To decide how to implement and tune these effects in our model, we turned to the experimental literature. Two studies reported on short-term plasticity of GPe and Str projections in *in vitro* slice preparations (***Connelly et al., 2010***; ***Lavian and Korngreen, 2016***). Because this data was averaged over multiple neurons and trials, we incorporated an established mean-field model of short-term synaptic depression/facilitation (***Abbott et al., 1997***; ***Dayan and Abbott, 2001***; ***Morrison et al., 2008***) into our simulated synaptic currents to capture short-term synaptic dynamics in our simulations.

Interestingly, the two experimental papers reported results that superficially appear to be at odds with each other. In ***Connelly et al.*** (***2010***), the magnitude of synaptic depression and facilitation of synapses onto SNr neurons was found to be largely independent of the tested stimulation frequencies ($10\,Hz$, $50\,Hz$, $100\,Hz$). In contrast, in a BG output nucleus analogous to the SNr, the entopeduncular nucleus (EP), a similar characterization of the short-term synaptic dynamics of GPe and Str projections found that short-term depression and facilitation are highly frequency-dependent (***Lavian and Korngreen, 2016***). Moreover, the magnitude of synaptic facilitation of Str projections was shown to decrease in the EP for simulation frequencies above $10\,Hz$.

A critical distinction between these studies is that data was collected under a voltage-clamp configuration in ***Connelly et al.*** (***2010***) and under a current-clamp configuration in ***Lavian and Korngreen*** (***2016***). Under current-clamp, the membrane potential (V_m) is free to change. Consequently, stimulation of GPe or Str projections hyperpolarizes V_m towards the GABAergic reversal potential (E_{GABA}), which reduces the GABAergic driving force ($V_m - E_{GABA}$) and ultimately decreases the magnitude of the inhibitory postsynaptic potential (IPSP). In contrast, the GABAergic driving force does not change under voltage-clamp, as V_m is fixed. In both voltage- and current-clamp E_{GABA} may also be considered fixed due to the whole cell configuration and free ionic diffusion between the cell and recording pipette. Based on these considerations, we tuned our model to match the voltage-clamp

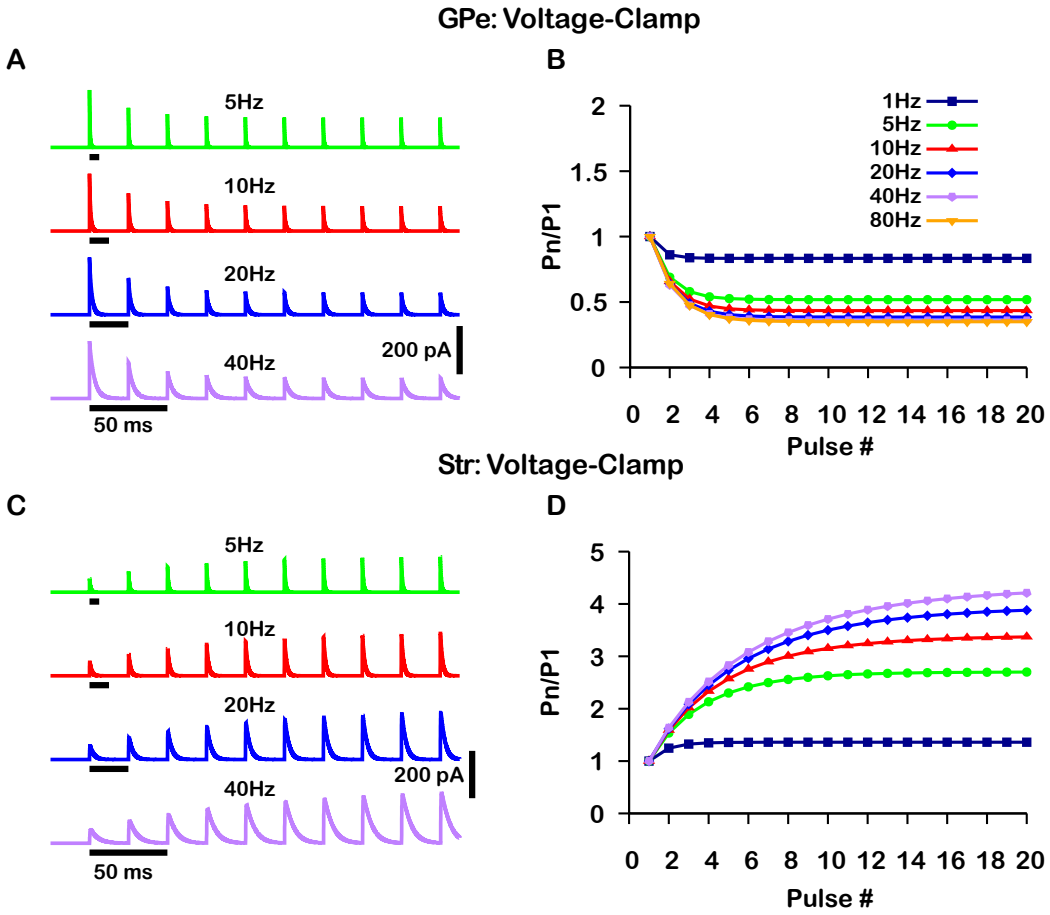

Figure 2. Simulated short-term synaptic depression and facilitation of GABAergic synapses originating from GPe neurons of the indirect pathway (A & B) and Str neurons of the direct pathway (C & D) under voltage clamp. For the GPe and Str simulations, the left traces (A & C) show current and right panels (B & D) show the pared pulse ratios (PPR) resulting from repeated synaptic stimulation at different frequencies. The amplitude of each IPSC (P_n) was normalized to the amplitude of the first evoked IPSC (P_1). For this set of simulations the membrane potential was held at $V_S = -60.0\,mV$ and E_{GABA} for the somatic and dendritic compartments was held fixed at $-72\,mV$. Model parameters and behavior were tuned to match voltage-clamp data from (***Connelly et al., 2010***).

data from ***Connelly et al.*** (***2010***), as it is likely a better representation of the underlying short-term synaptic dynamics of GPe and Str inputs (Fig. 2). Interestingly, with this tuning, the short-term GPe and Str synaptic dynamics in our model when tested under current-clamp also reproduces the synaptic dynamics reported in ***Lavian and Korngreen*** (***2016***). Specifically, GPe synaptic depression and Str synaptic facilitation are strongly frequency dependent, and the magnitude of synaptic facilitation in Str synapses decreases for stimulation frequencies above $10\,Hz$ (Fig. 3). These results demonstrate the importance of considering the differences between voltage- and current-clamp recordings when characterizing short-term synaptic dynamics. Additionally, these findings suggest that short-term synaptic dynamics of inputs from GPe and Str in the EP are tuned in a similar way to those in the SNr.

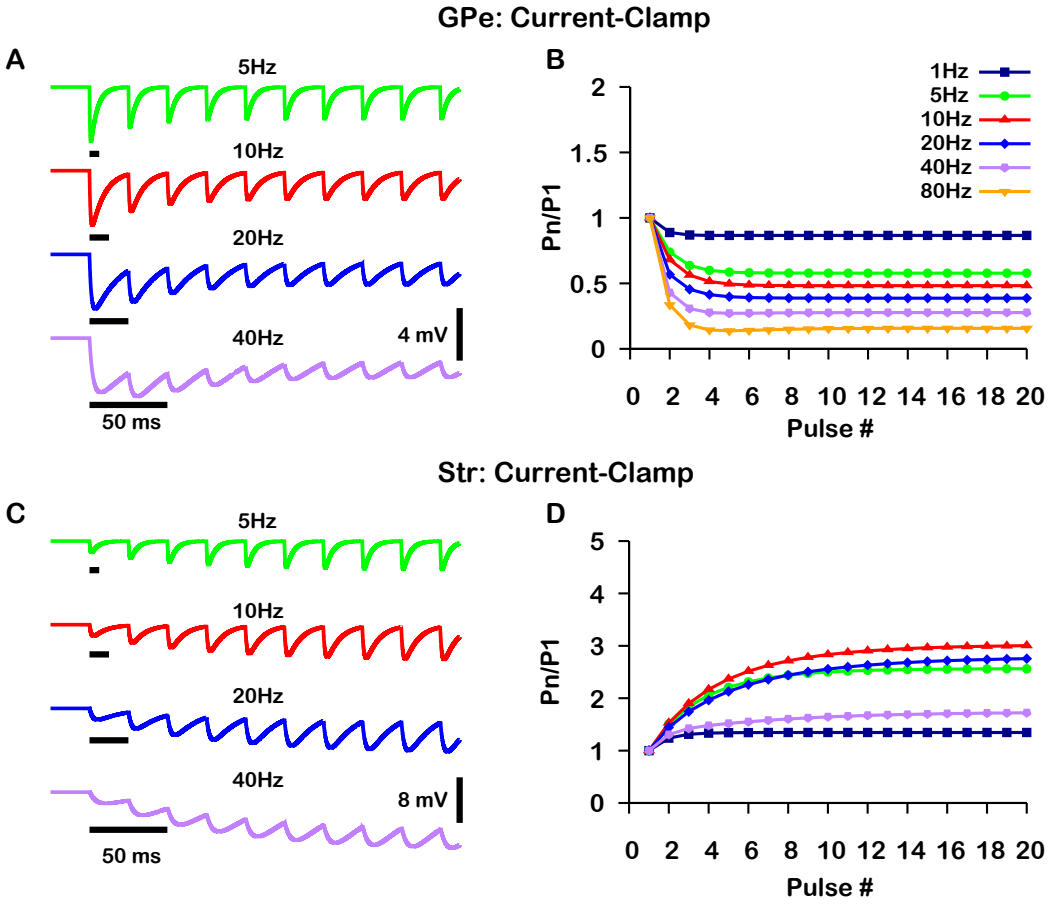

Figure 3. Simulated short-term synaptic depression and facilitation of GABAergic synapses originating from GPe neurons of the indirect pathway (A & B) and Str neurons of the direct pathway (C & D) under current clamp. For the GPe and Str simulations, the left traces (A & C) show voltage and right panels (B & D) show the pared pulse ratios (PPR) resulting from repeated synaptic stimulation at different frequencies. The amplitude of each IPSP (P_n) was normalized to the amplitude of the first evoked IPSP (P_1). For this set of simulations the I_{APP} applied inorder to set the resting membrane of the somatic compartment at $V_S = -60.0\,mV$. In both compartments E_{GABA} was held fixed at $-72\,mV$. Model performance is qualitatively, and somewhat quantitatively, similar to experimental current-clamp data ((***Lavian and Korngreen, 2016***), Figs. 2-3).

SNr responses to simulated stimulation of GPe and Str inputs depend on E_{GABA} and intracellular Cl^- levels

Next, we used our model to consider effects of variability of the GABA reversal potential on SNr responses to its GABAergic inputs. Maintenance of the Cl^- gradient is largely determined by a neuron's ability to preserve a low intracellular chloride concentration ($[Cl^-]_i$), which in turn depends on the balance of the neuron's capacity for Cl^- extrusion by the potassium-chloride co-transporter KCC2 (***Doyon et al., 2011***; ***Raimondo et al., 2012***; ***Doyon et al., 2016b***; ***Mahadevan and Woodin, 2016***) and the Cl^- influx into the neuron that occurs through Cl^--permeable ion channels that contribute to I_{GABA}.

Due to the importance of Cl^- regulation in GABAergic synaptic transmission, we first characterized the relationship among a conductance associated with a tonic chloride load (g_{GABA}^{Tonic}), the Cl^- extrusion capacity (g_{KCC2}), and E_{GABA} in the somatic compartment of our model (Fig. 4 A). We found that E_{GABA} may vary from approximately $-80\,mV$ with very low net Cl^- influx to approximately $-45\,mV$ with high g_{GABA}^{Tonic} and low Cl^- extrusion capacity (note that the level of depolarization of E_{GABA} is also influenced by the HCO_3^- concentration gradient across the cell membrane (***Kaila***

and Voipio, 1987; *Kaila et al., 1989*; *Staley et al., 1995*; *Staley and Proctor, 1999*; *Raimondo et al., 2012*); see Methods, Eq. 23). Importantly, depending on g_{GABA}^{Tonic} and g_{KCC2}, E_{GABA} can vary over ranges that correspond to excitatory, inhibitory and shunting effects of the resulting GABAergic current even for relatively small g_{GABA}^{Tonic}.

Next, we investigated the effect of simulated somatic GABAergic projections from the GPe on the firing rate of the model SNr neuron. This was achieved by simulating optogenetic stimulation of the model's somatic synapses at $40\,Hz$ for $1\,s$. Four distinct types of SNr firing rate responses were observed: "complete inhibition", "no effect", "excitation", and "partial inhibition" (Fig. 4 B-E). Additionally, two sub-types of partial inhibition occurred: (1) deletion of one or a few spikes deletion followed by a step reduction in firing rate (Fig. 4 E1) and (2) complete inhibition followed by a late escape and continuation of spiking (Fig. 4 E2). The type of response in the model depends on the magnitude of E_{GABA} relative to V_m at the start of the stimulation, and, in the case of the second type of partial inhibition, the slow depolarizing drift of E_{GABA} that is the result of intracellular Cl^- accumulation. The effects of the short-term synaptic depression at these synapses on most of the SNr responses turns out to be minimal. This lack of effect arises because these synapses a reach steady-state level of depression after approximately five stimulus pulses, which occurs after just $125.0\,ms$ when stimulating at $40\,Hz$. The one exception occurs with the first type of partial inhibition, for which g_{GABA} is large enough at the start of the stimulation window to cause an early spike deletion, after which depression can allow the reduced-rate firing to emerge.

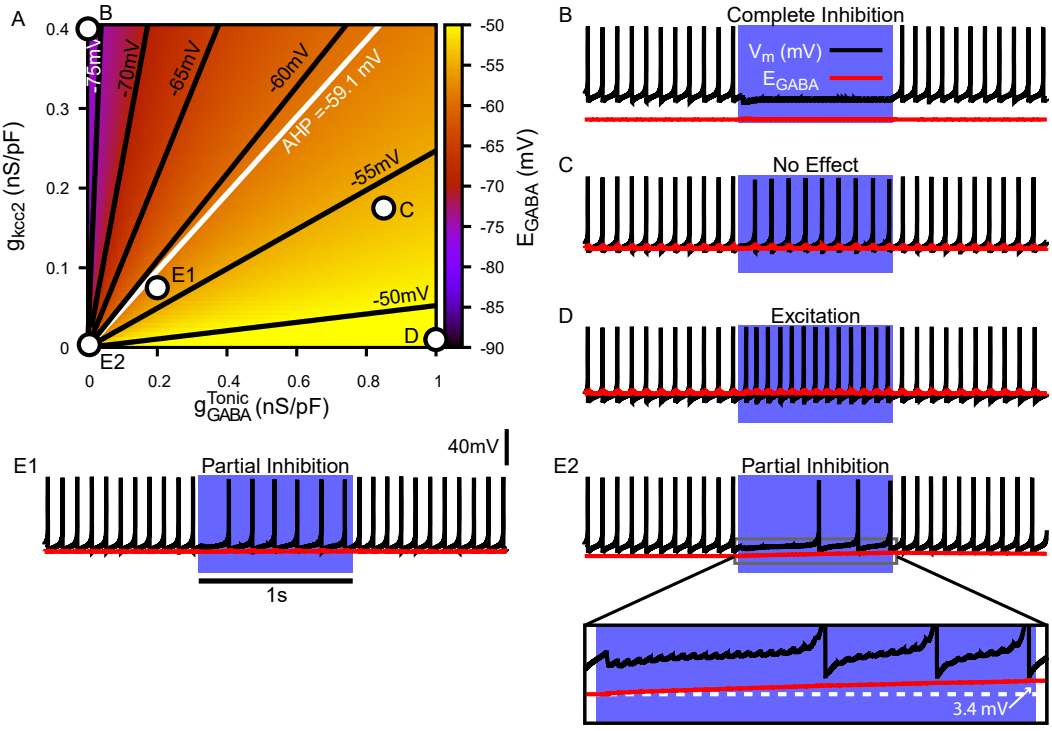

Figure 4. Tonic chloride conductance and extrusion capacity determine somatic E_{GABA} and SNr responses to simulated $40\,Hz$ GPe stimulation. (A) Dependence of somatic E_{GABA} on the tonic chloride conductance (g_{GABA}^{Tonic}) and the potassium-chloride co-transporter KCC2 extrusion capacity (g_{KCC2}). (B-E) Examples of SNr responses to simulated indirect pathway stimulation at different positions in the 2D (g_{GABA}^{Tonic},g_{KCC2}) parameter space, as labeled in the top left panel. (E1 & E2) Notice the two distinct types of partial inhibition. Inset highlights the drift in E_{GABA} during stimulation.

We next performed a parallel analysis of the effects of simulated optogenetic stimulation of Str GABAergic projections in the dendritic compartment of the SNr model under the same stimulation protocol. As with the somatic compartment, we first characterized the relationship among g_{GABA}^{Tonic}, g_{KCC2} and E_{GABA} in the dendritic compartment and found that E_{GABA} varies over a comparable range ($-80\,mV$ to $-45\,mV$), depending on the balance of Cl^- influx and extrusion rates (Fig. 5 A). Stimulation of the dendritic GABAergic synapses resulted in the same four response types seen in the somatic compartment with an additional "biphasic inhibitory-to-excitatory" response and a slightly different pair of "partial inhibition" responses (Fig. 5 B-F), one mediated by the short-term facilitation of direct pathway synapses. Specifically, with repeated stimulation, the strengthening of these synapses can induce a gradual slowing in the SNr firing rate throughout the simulation, which may eventually stop neuronal spiking (Fig. 5 E1). Despite this facilitation, a form of partial inhibition consisting of an initial pause in SNr spiking followed by a recovery of spiking can also occur in the model with direct pathway stimulation, mediated by a sufficiently large Cl^- accumulation to allow the effects of dynamic E_{GABA} to dominate the post-synaptic response (Fig. 5 E2). The biphasic inhibitory-to-excitatory response type is an extreme case of the partial inhibition shown in Fig. 5 E2. This biphasic response occurs when E_{GABA} is initially hyperpolarized relative to V_m, the Str GABAergic conductance is strong and the Cl^- extrusion capacity is weak, which allows for unusually rapid Cl^- accumulation and subsequent depolarization of E_{GABA} near or above the action potential threshold. The biphasic response type is predicted to occur with Str but not GPe stimulation, due to the larger surface area-to-volume ratio and concomitant increased susceptibility to Cl^- accumulation in the dendritic compartment that Str inputs target, relative to the soma.

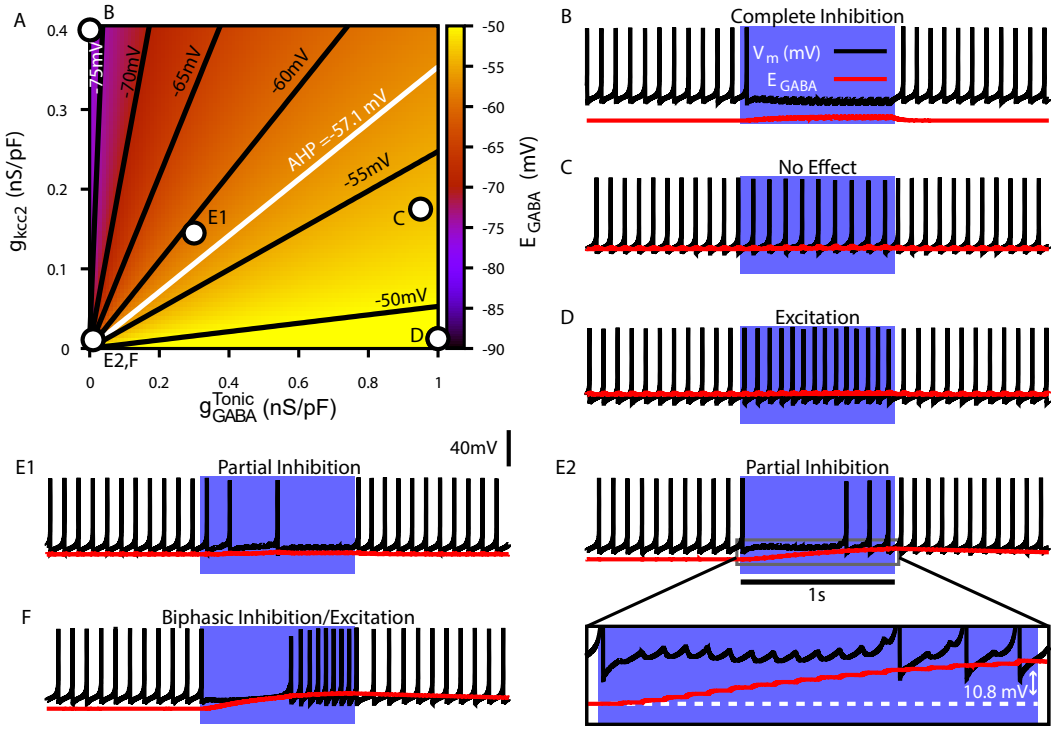

Figure 5. Tonic chloride conductance and extrusion capacity determine dendritic E_{GABA} and SNr responses to $20\,Hz$ Str stimulation. (A) Dependence of somatic E_{GABA} on the tonic chloride conductance (g^{Tonic}_{GABA}) and the potassium-chloride co-transporter KCC2 extrusion capacity (g_{KCC2}). (B-F) Examples of SNr responses to simulated indirect pathway stimulation at different locations in the 2D (g^{Tonic}_{GABA},g_{KCC2}) parameter space. g^{Tonic}_{GABA} and g_{KCC2} for each example are indicated in the top left panel. (E1 & E2) Notice the two distinct types of partial inhibition. Inset highlights the drift in E_{GABA} during stimulation. (F) Example of a biphasic inhibition-to-excitation response elicited by increasing the stimulation frequency to $40\,Hz$ under the same conditions shown in E2. Alternatively, same response could be elicited by increasing the synaptic weight (W^{Str}_{GABA}).

Optogenetic stimulation of GPe and Str GABAergic synaptic terminals in the SNr results in diverse neuronal responses

Our simulations in the previous sections predict that GABAergic inputs from the GPe and Str may produce a diverse range of effects on SNr activity depending on E_{GABA} and $[Cl]_i$ levels and dynamics. To test these predictions, we optogenetically stimulated the synaptic terminals from D1 striatal neurons of the direct pathway and from GPe neurons of the indirect pathway in the SNr for $10\,s$ periods. During stimulation, we performed patch clamp recordings of SNr activity. Experiments were conducted in *in vitro* slice preparations and patch clamp recordings were performed in cell attached mode to avoid perturbing the intracellular Cl^- concentration critical for GABAergic signaling. In response to optogenetic stimulation, we found a wide array of SNr response types, which we classified into five categories: (1) complete inhibition - cessation of spiking; (2) partial inhibition - sufficient reduction of firing rate with or without a pause; (3) no effect - no change in firing rate; (4) excitation - sufficient increase in firing rate; and (5) biphasic - decrease or pause in spiking followed by an increase in firing rate above baseline. Example traces for the response types observed with GPe and Str stimulation are shown in Fig. 6A1 & B1, and the frequencies of occurrence for these responses are quantified in Fig. 6A2 & B2; see also Supplemental Figures S1 and S2 for raster plots and firing rate time courses for all frequencies tested. All response types could be induced by optogenetic stimulation of the GPe or the Str projection; however, with GPe stimulation, biphasic responses were slower to emerge (see Supplemental Figure S1) and less common overall

than with Str stimulation, consistent with the absence of biphasic responses in our $1\,s$ simulations of GPe inputs and with slower Cl^- accumulation, over several seconds, in the soma than in the dendrite. In a portion of the neurons partially inhibited by GPe or Str stimulation, the duration of the pause in spiking is longer than can be explained by short-term synaptic dynamics. Additionally, the number of partially inhibited neurons with a "long pause" increases with stimulation frequency (GPe:$10\,Hz, 1/25$; $20\,Hz, 8/26$; $40\,Hz, 13/29$; $60\,Hz, 16/24$; Str:$10\,Hz, 1/25$; $20\,Hz, 8/26$; $40\,Hz, 13/29$; $60\,Hz, 16/24$). Moreover, the strength of GPe and Str synaptic inhibition gradually decreased over the $10\,s$ stimulation period Fig. 6A3 & B3. These findings, in addition to the observation of biphasic responses, are consistent with gradual Cl^- accumulation and depolarization of E_{GABA} during the stimulation period.

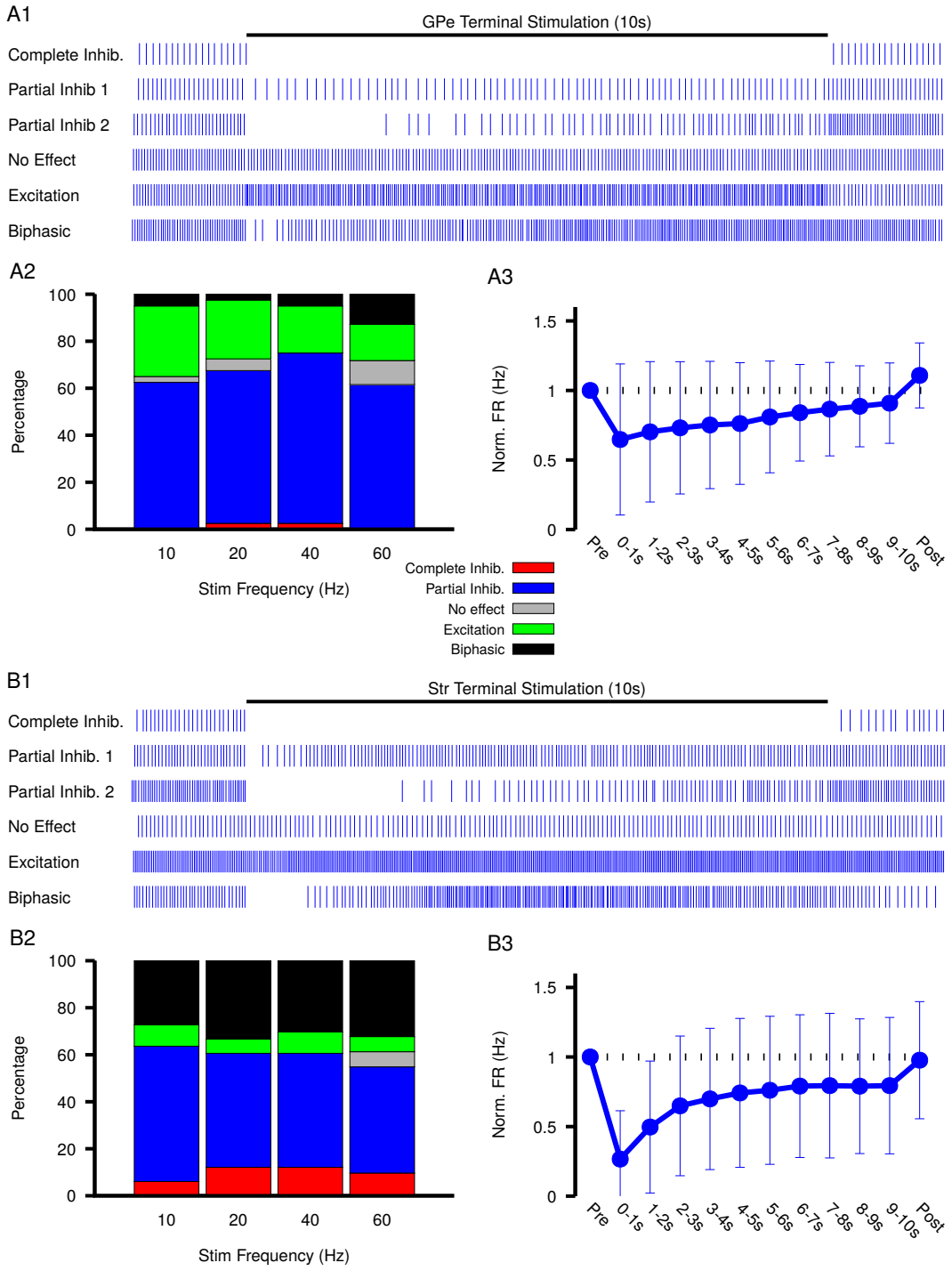

Figure 6. Characterization of experimentally observed SNr responses to optogenetic stimulation of (top) GPe and (bottom) Str projections to SNr *in vitro*. (A1 & B1) Examples of response types observed for 10s stimulation of GPe or Str projections. (A2 & B2) Quantification types of SNr response to optogenetic stimulation at varying frequencies. (A3 & B3) Effect of GPe or Str stimulation on the firing rate of SNr neurons averaged across all trials for stimulation at $40\,Hz$. Error bars indicate the standard deviation. The $10\,s$ stimulation period was broken into $1\,s$ intervals to show the gradual weakening of inhibition during stimulation.

Previous computational modeling studies that have shown that, due to the larger surface area-to-volume ratio of dendrites relative to the soma, Cl^- accumulation and depolarization of E_{GABA} is faster in dendritic compared to somatic compartments (***Doyon et al., 2011***; ***Ratté and Prescott, 2011***), and this result could explain why biphasic responses were only seen with Str stimulation. Nonetheless, Cl^- accumulation and depolarization of E_{GABA} may still arise, on a slower time scale, with stimulation of the indirect pathway. If slow Cl^- accumulation and depolarization of E_{GABA} are indeed occurring, then the strength of inhibition should slowly weaken during stimulation, which will result is a slow increase in firing rate during the stimulation period.

Measurements of spiking frequency relative to baseline during and after stimulation of the GPe and Str projections as a function of stimulation frequency (Fig. 6E & F) support the idea that E_{GABA} dynamics may contribute to synaptic integration within the SNr. For this analysis, we divided the stimulation period into thirds in order to assess any dynamic changes in the strength of the input over the course of stimulation. We found that Str projections are initially more effective at inhibiting SNr spiking relative to GPe projections (Str: $72.3 - 76.7\%$ peak reduction, GPe: $43.1 - 61.9\%$ peak reduction). Interestingly, for both GPe and Str projections, the strength of inhibition decreases on average during the stimulation period, consistent with slow accumulation of intracellular chloride. Moreover, the loss of firing rate reduction was most prominent for Str stimulation at high frequency, despite short-term synaptic facilitation known to occur at these synapses (***Connelly et al., 2010***; ***Lavian and Korngreen, 2016***), consistent with the emergence of some excitatory and biphasic SNr responses in that regime.

The diversity of experimental responses to GPe and Str stimulation seen in Fig. 6 support the idea that GABAergic synaptic transmission in the SNr is not purely inhibitory and may even be excitatory in some neurons. In the following sections we return to our computational model to explore the functional significance of this finding in physiologically relevant settings.

E_{GABA} tunes local SNr synchrony and may promote slow oscillations

In addition to receiving GABAergic projections from the GPe and Str, SNr neurons interact locally through $GABA_A$-mediated synaptic transmission (***Mailly et al., 2003***; ***Brown et al., 2014***; ***Higgs and Wilson, 2016***). The role of these synapses is unclear; however, they have been proposed to regulate synchronization of SNr activity (***Higgs and Wilson, 2016***). Levels of E_{GABA} will affect the strength and polarity (inhibitory, shunting, excitatory) of these interactions. Therefore, we next used our computational model to characterize how variations in E_{GABA}, potentially due to differences in GPe firing rates, affect these local SNr interactions.

On average, a given SNr neuron receives GABAergic synaptic projections from 1-4 neighboring SNr neurons (***Higgs and Wilson, 2016***). Consequently, synaptic interactions between SNr neurons result in brief synaptic transients that have been proposed to impact neuronal synchrony incrementally by changing the oscillatory phase of the post-synaptic neuron. Therefore, we first characterized how transient GABAergic stimulation modulates the phase of our model SNr neuron as a function of the phase of the SNr oscillation at which the stimulation occurs, using phase response curves (PRCs) (***Ermentrout, 1996***; ***Ermentrout and Terman, 2010***) computed for an array of values of E_{GABA} (see Fig. 7). The PRCs that we obtained for hyperpolarized values of E_{GABA} are qualitatively consistent with those found previously for mouse SNr neurons in brain slices with $E_{GABA} \approx -65mV$ (***Simmons et al., 2018***).

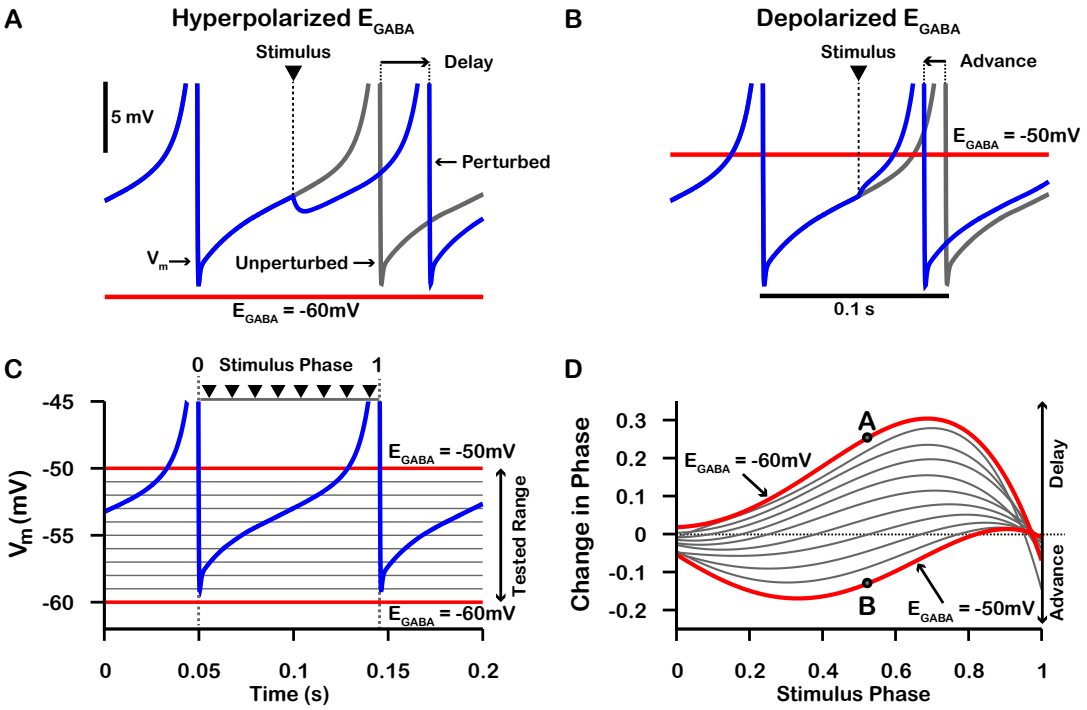

Figure 7. Phase response curves (PRCs) of the model SNr neuron depend on E_{GABA}. (A & B) Example traces illustrating the effect of a single GABAergic synaptic input on the phase of spiking in a simulated SNr neuron for hyperpolarized and depolarized E_{GABA}, respectively. (C) For an ongoing voltage oscillation of a spiking SNr neuron (blue trace), we define a phase variable as progressing from 0 immediately after a spike to 1 at the peak of a spike. As E_{GABA} is varied from $-60\,mV$ to $-50\,mV$, progressively more of the SNr voltage trace lies below E_{GABA}, where GABAergic inputs have depolarizing effects. (D) PRCs computed for a model SNr neuron in response to GABAergic input stimuli arriving at different phases of an ongoing SNr oscillation. As E_{GABA} is varied from $-60\,mV$ to $-50\,mV$, the PRC transitions from a curve showing a delay of the next spike for most stimulus arrival phases, through some biphasic regimes, to a curve showing an advance of the next spike for almost all possible phases. In panel D, the A and B labels at approximately 0.5 phase on the $E_{GABA} = -60\,mV$ and $E_{GABA} = -50\,mV$ PRCs correspond to the examples shown in panels A and B. The conductance of the synaptic input was fixed at $0.1\,nS/pF$ in order to produce deflections in V_m for hyperpolarized E_{GABA} that are consistent with data presented in ***Higgs and Wilson* (*2016*)**.

PRCs can be used to predict the synchrony between two oscillating neurons that interact synaptically (***Ermentrout, 1996***; ***Jeong and Gutkin, 2007***; ***Ermentrout and Terman, 2010***; ***Smeal et al., 2010***). We applied this idea with our computationally-generated PRCs to predict the synchrony in a network of two SNr neurons under two configurations, unidirectional and bidirectional synaptic connectivity (Fig. 8). For the unidirectional case a first, presynaptic SNr neuron stimulates a second, postsynaptic one. Phases of the presynaptic neuron's ongoing oscillation at which the firing of the postsynaptic neuron will become locked can be predicted by finding locations where the PRC crosses the horizontal (phase) axis. Although all crossings represent fixed points and hence phases at which locking can theoretically occur, only those with a positive slope are stable and are predicted to arise robustly and be observed in simulations (e.g., (***Ermentrout, 1996***; ***Ermentrout and Terman, 2010***)). By tracking the fixed points, we found that in the unidirectional case, the locked phase relation between the two SNr neurons is predicted to go from synchrony, or phase 0, to progressively more asynchronous phase locking and then back toward synchrony again as E_{GABA} depolarizes from $-60\,mV$ to $-50\,mV$, with perfectly anti-phase spiking for $E_{GABA} \approx -53\,mV$ (Fig. 8 A4). We also observe that phase locking is predicted to be unstable (indicated by open circles) for sufficiently negative E_{GABA} (less than $\approx -57\,mV$).

To test these predictions computationally, we simulated the unidirectionally connected two-

neuron network and recorded difference in the timing of spikes in neuron 2 relative to the phase of neuron 1 (phase difference). We found that the predicted synchrony/asynchrony is in good agreement with our simulations, and is indicated by the distributions of phase difference histograms shown in Fig. 8 A4 (gray curves). Interestingly, for relatively hyperpolarized E_{GABA} where synchronous phase locking is predicted to be unstable we observe that, instead of phase locking, slow oscillations in the phase of the postsynaptic neuron relative to that of presynaptic neuron begin to emerge. Correspondingly, the distribution of presynaptic neuron phases when the postsynaptic neuron fires spreads out across the [0,1] interval and the frequency of firing of neuron the postsynaptic neuron repeatedly drifts below that of the presynaptic neuron, at a rate of about $1\ Hz$ (Fig. 8 A5). The mechanism underlying these slow oscillations will be discussed in more detail below.

For bidirectional connectivity, we no longer have a clear distinction between a pre- and a postsynaptic neuron, and instead we just refer to neuron 1 and neuron 2. Due to the symmetry of the network, we can plot the PRC for neuron 1 together with that of neuron 2 by reflecting the PRC for neuron 2 about the mid-point of the phase axis, 0.5 (see Methods for more detail). Phase locking between the two neurons can then be predicted by finding the intersections (fixed points) of these two PRCs (Fig. 8 B1-B3). By symmetry, approximately 0.5 is always a fixed point in this case, and we found that this was the only fixed point for the bidirectional system and remained stable regardless of the value of E_{GABA} (Fig. 8B1-4). Again, this prediction was tested by simulating the bidirectionally connected two-neuron network and recording the phase difference between the two neurons. The predicted asynchrony between the two neurons is in good agreement with our simulations, in which the phase difference between the two neurons remained tightly distributed around 0.5 for all values of E_{GABA} tested (Fig. 8 B4).

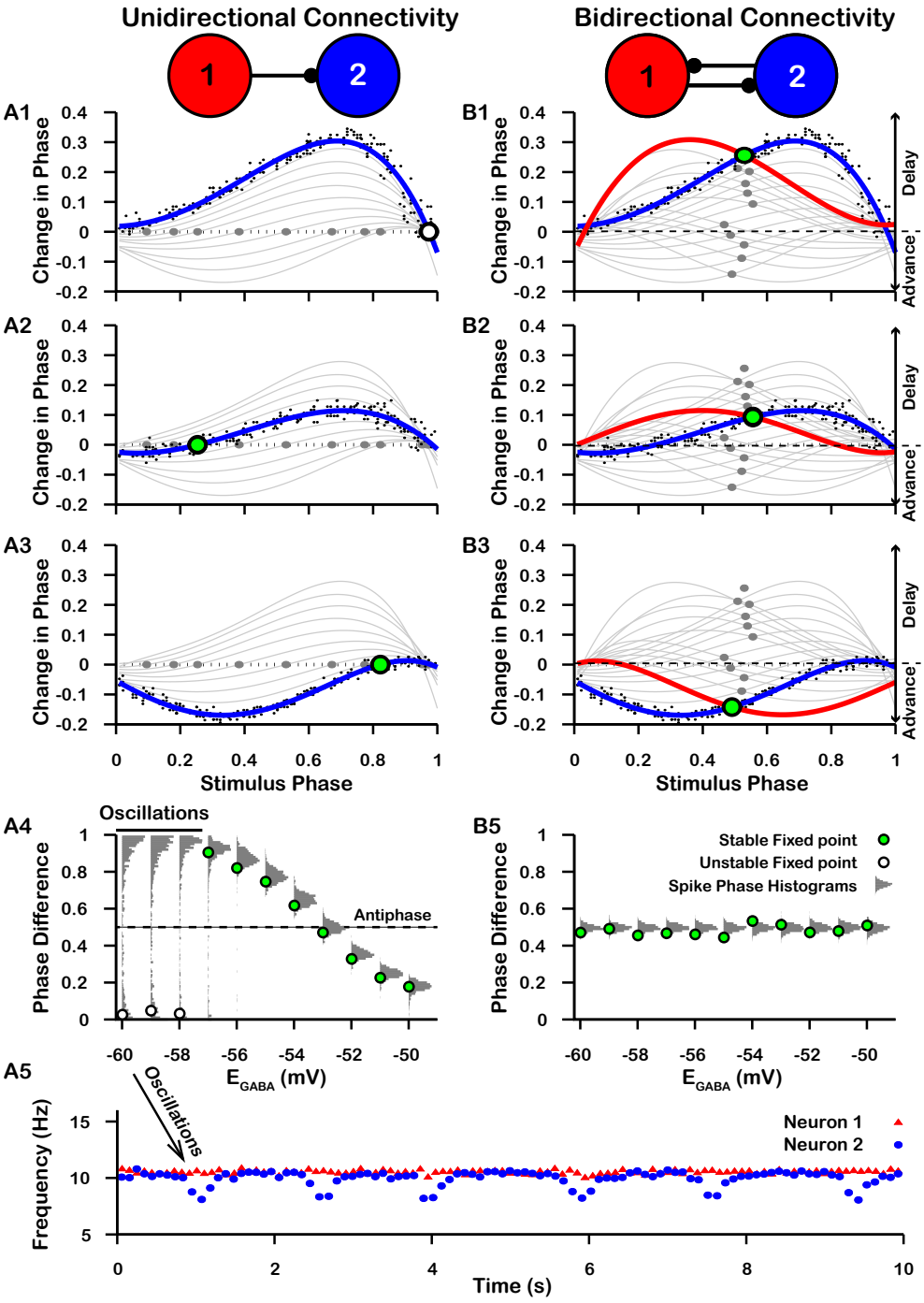

Figure 8. Effect of E_{GABA} on SNr synchrony in a unidirectional (left) and bidirectional (right) synaptically connected two-neuron network. (A1-A3 & B1-B3) Identification of PRC fixed points as a function of E_{GABA}. *Recall that positive changes in phase correspond to delays.* (A1,B1) $E_{GABA} = -60\,mV$; (A2,B2) $E_{GABA} = -56\,mV$; (A3,B3) $E_{GABA} = -50\,mV$. Black dots indicate dataset used to generate PRC in red/blue. Stable and unstable fixed points are indicated by green and white filled circles, respectively. For reference, all PRCs and fixed points are included in gray for all values of E_{GABA} tested. (A4,B4) Effect of E_{GABA} on SNr phase locking. Gray histograms show the distribution of the difference in the timing of spikes in neuron 2 relative to the phase of neuron 1 (phase difference) for the two network simulations for different levels of E_{GABA}. Green and white filled circles indicate the stable and unstable locking predicted by analysis of PRCs. Note the unstable fixed points for the lowest values of E_{GABA} in the unidirectional case. (A5) In the unidirectional case, slow $1\,Hz$ oscillations in the frequency of neuron 2 arise due to phase slipping at hyperpolarized values of E_{GABA}.

The slow oscillations of approximately $1\,Hz$ seen with unidirectional connectivity can be understood by taking a closer look at the PRCs calculated for E_{GABA} less than approximately $-57\,mV$ in the undirectional case (Fig. 8 A). For these values of E_{GABA}, the PRCs only have unstable fixed points.Under these conditions, the phase of neuron 2 relative to neuron 1 is delayed by different amounts across successive inputs from neuron 2 (or possibly advanced if inputs arrive during a specific narrow phase window). Moreover, based on the shape of the PRC, the magnitude of change in phase is large when phase is away from 0 and 1, such that spiking is asynchronous, and small when the phase of is nearly synchronous. As a result, the network remains close to synchrony most of the time but with approximately periodic asynchronous excursions, a phenomenon referred to as phase slipping (***Thounaojam et al., 2014***). The frequency of phase slipping is determined by the number of stimulus kicks needed for the phase to progress through one full cycle, which in turn is determined by the shape of the PRC. For example, one full phase slipping cycle is illustrated in Fig. 9 A-B for $E_{GABA} = -60\,mV$. As previously mentioned, the slow oscillation in phase is also seen as a periodic negative excursion in the frequency of spiking (Fig. 8 A5).

Finally, since the frequency of phase slipping oscillations is determined by the shape of the PRC and the PRC is in part determined both by E_{GABA} and by the weight/conductance of the synaptic projection from the other neuron (W_{GABA}^{SNr}), changes in E_{GABA} or W_{GABA}^{SNr} should affect the phase slipping frequency. Therefore, we also characterized the relationship between E_{GABA} and the frequency of the phase slipping for different values of W_{GABA}^{SNr}. In our simulations, we found that phase slipping oscillations begin at approximately $E_{GABA} = -56\,mV$ and linearly increase in frequency as E_{GABA} is held at progressively more hyperpolarized values (Fig. 9 C). The hyperpolarization of E_{GABA} leads to stronger inhibition and hence a larger PRC amplitude, which allows for the postsynaptic neuron to progress through the full phase range on fewer cycles (i.e., at a higher frequency). Moreover, the slope of the linear relationship between E_{GABA} and frequency increases/decreases with increases/decreases in the strength of W_{GABA}^{SNr} due to similar effects. We also simulated SNr neurons with different levels of applied current, leading to different firing rates, but this variability did not strongly impact resulting oscillation frequencies.

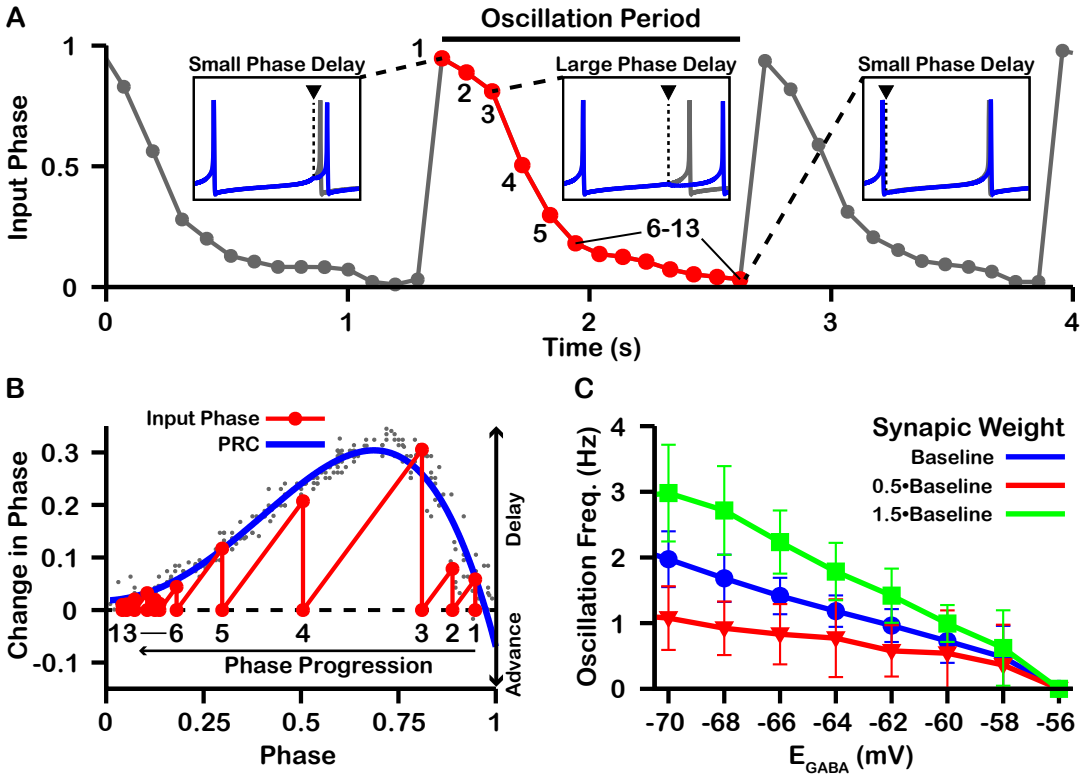

Figure 9. Characterization of phase slipping oscillations in the unidirectionally connected two-neuron network. (A) Illustration of the phase of the postsynaptic neuron at the moment when it receives each input from the presynaptic neuron (input phase) for the unidirectionally connected two neuron network as a function of time for $E_{GABA} = -60\,mV$. Dots denote phases of the presynaptic neuron when the postsynaptic neuron spikes. The phase value of 1 corresponds to the postsynaptic neuron being at spike threshold. Insets show the timing of the presynaptic neuron spike (black triangle/dashed line), the phase of the postsynaptic neuron spike after it receives the input (blue), and the spike train of the postsynaptic neuron in the absence of input (gray). The red cycle is used in B. (B) Overlay of the PRC generated for $E_{GABA} = -60\,mV$ and the resulting progression of phase for one full phase slipping oscillation. Light gray dots indicate the data points used to generate the blue PRC. Recall that positive changes in phase correspond to delays. (C) The frequency of phase slipping increases as E_{GABA} decreases, with a steeper relationship for larger synaptic weight (W_{GABA}^{SNr}) between the SNr neurons.

.

Optogenetic stimulation of GPe neurons suppresses SNr oscillations

Slow oscillations have been reported in the SNr *in vivo* under dopamine depleted (DD) conditions in lightly anaesthetized (***Walters et al., 2007***) and awake behaving animals (***Whalen et al., 2020***). Our simulations predict that similar slow oscillations will occur when E_{GABA} is equal to or hyperpolarized relative to the membrane AHP. Assuming that these oscillations are driven by the mechanism described in Fig. 9, manipulations that depolarize E_{GABA} should reduce and stop such oscillations. As illustrated in Fig. 4, changing the tonic Cl^- conductance to the soma is one way to depolarize E_{GABA}. This could be achieved by increasing the firing rate of GPe neurons. Therefore, next we examined if these slow oscillations are suppressed by optogenetic stimulation of GPe neurons in the SNr. Consistent with previous descriptions (***Walters et al., 2007***; ***Whalen et al., 2020***), under DD conditions we found slow oscillations in the firing rates of SNr neurons (Fig. 10 A-C). The frequency of the oscillations was characterized by finding the peak in the power spectral density (PSD) as described in ***Whalen et al.*** (***2020***) and shown in Fig. 10 B. We identified five oscillatory units with frequencies ranging from $1.46\,Hz$ to $1.95\,Hz$ (mean $\pm$ SD = $1.7 \pm 0.204\,Hz$, Fig. 10 C). In these units, optogenetic stimulation of GPe terminals in the SNr had limited effect on SNr firing rates during a $30\,s$ stimulation period (Fig 10 D; see *Materials and Methods* for a full description of the experimental

preparation and stimulation protocol). Yet, stimulation of GPe terminals in the SNr significantly reduced the power in the PSD in the 0.25-4.0 Hz band (Fig. 10 E). The impact of GPe stimulation on oscillations but not firing rate in the SNr is consistent with our simulations and suggests that slow oscillations in the SNr seen under DD conditions may be due to the phase slipping mechanism described in Fig. 9. These data also suggest that a role of the GPe may be to tune SNr dynamics by modulating the tonic Cl^- conductance and E_{GABA} in the SNr.

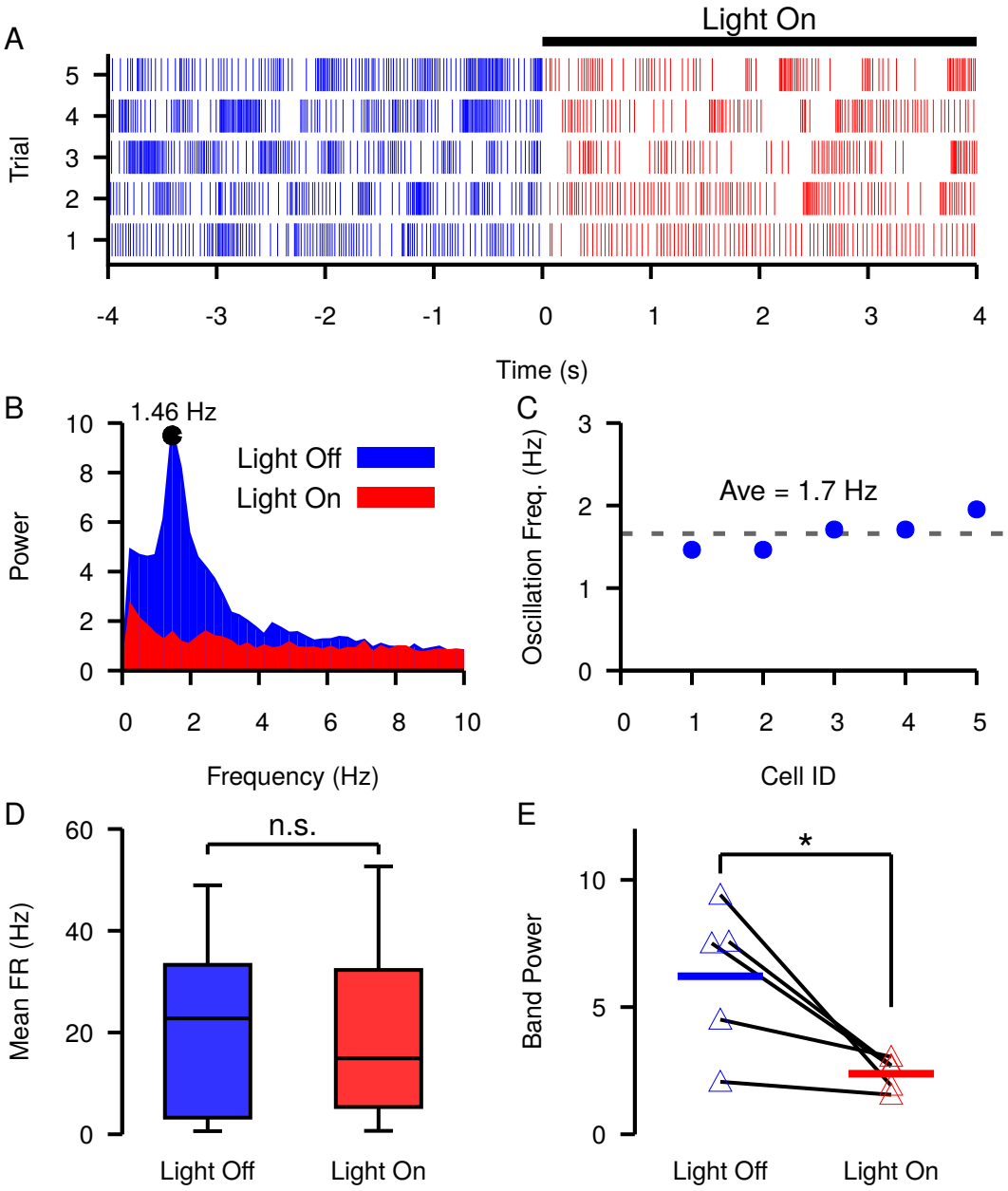

Figure 10. Slow oscillations in the SNr seen under dopamine depleted conditions *in vivo* are suppressed by channelrhodopsin-2 optogenetic stimulation of GABAergic GPe terminals in the SNr. (A-B) Example (A) raster plot and (B) power spectrum of a single spiking unit in SNr without (blue) and with (red) optogenetic stimulation of GPe terminals over multiple trials. (C) Frequencies of slow oscillations in the 12 unit dataset before optogenetic stimulation. (D) Distribution of single unit firing rates without (blue) and with (red) optogenetic stimulation for all recorded units (n=12). Notice that stimulation has no significant effect on firing rate (t-test p=0.8531). (E) Band power ($0.75 - 3.0\ Hz$) without (blue) and with (red) optogenetic stimulation for oscillatory units (n=5). Solid blue and red horizontal bars indicate mean band power. Notice that stimulation significantly reduces the power of the slow oscillations (t-test p=0.0341).

.

337 **E_{GABA} tunes the strength of direct pathway inhibition and may affect response**
338 **times in perceptual decision-making tasks**

339 In tasks involving perceptual decision-making, visual motor responses (saccades) are thought to be
340 triggered when evidence accumulates above some threshold level. Experiments suggest that the

BG is involved is regulating the dynamics of these visual motor responses (***Basso and Wurtz, 2002***; ***Basso et al., 2005***; ***Shires et al., 2010***; ***Sato and Hikosaka, 2002***). In the BG, evidence accumulation is thought to be represented by a ramping increase in the firing rate in striatal neurons of the direct pathway (***Ding and Gold, 2010***) that, above some threshold, generates a pause in SNr activity (***Wei et al., 2015***; ***Dunovan et al., 2019***). The pause in SNr spiking disinhibits downstream motor targets and allows the initiation of a selected action. As we have shown above, the effect(s) of striatal inputs on the firing rate and pattern of SNr neurons is highly dependent on E_{GABA}, which, in turn, is determined by the tonic chloride conductance and the Cl^- extrusion capacity of the KCC2 pump. Therefore, changes in E_{GABA} are predicted to modulate the threshold at which ramping striatal activity will generate a pause in SNr firing.

In the previous section we argued that the tonic GABAergic input from GPe neurons of the direct pathway may provide a mechanism to tune E_{GABA} in the soma of SNr neurons. Assuming that the coupling between the somatic and dendritic compartments is sufficiently strong, the tonic somatic Cl^- conductance provided by GPe inputs may also tune E_{GABA} in the dendritic compartment. To illustrate this idea, we first constructed a population of 100 SNr neurons with a baseline firing rate turned up to $\approx 25\,Hz$ in order to better represent *in vivo* conditions (***Freeze et al., 2013***; ***Mastro et al., 2017***; ***Willard et al., 2019***) (Fig. 11 A, B). In this set of simulations $[Cl]^-$ in the somatic and dendritic compartments interact by the addition of a coupling term (see Methods for a full description). Next, we characterized E_{GABA} in the somatic and dendritic compartments as a function of the tonic somatic Cl^- conductance (representing the tonic GABAergic GPe input). As expected, E_{GABA} depolarizes in both compartments as the somatic chloride conductance is increased (Fig. 11 C). In the dendritic compartment in particular, E_{GABA} ranges from just below $-75\,mV$ with no chloride conductance to approximately $-57\,mV$ with a $1.0\,nS/pF$ Cl^- conductance in the soma.

Finally, we characterized the relationship between tonic Cl^- conductance and the time required to decrease the mean SNr population firing rate below thresholds of $1\,Hz$, $5\,Hz$, and $10\,Hz$ in response to a ramping striatal input (Fig. 11 D-F). As the tonic Cl^- conductance increases, E_{GABA} becomes less hyperpolarizing (Fig. 5) and hence more time is needed to push SNr activity below threshold; for high enough Cl^- conductance, the ramping striatal input is unable to suppress SNr firing below $1\,Hz$. These simulations illustrate a plausible mechanism through which the tonic Cl^- conductance provided by the level of GPe activity may be able to tune dendritic (and somatic) E_{GABA}, altering SNr responses to direct pathway striatal inputs and, ultimately, the response times in perceptual decision-making tasks.

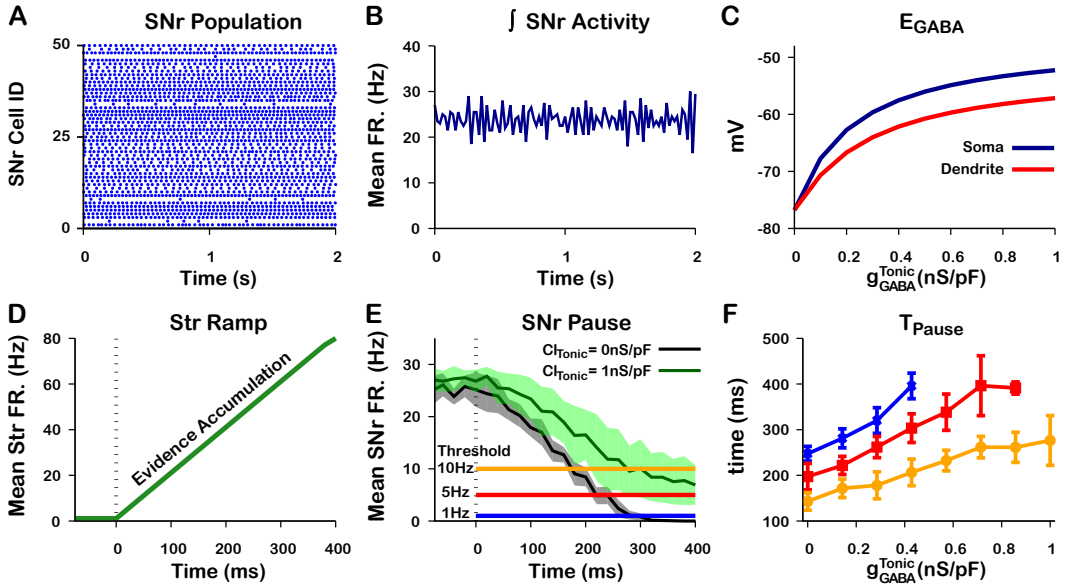

Figure 11. Tonic somatic Cl^- conductance affects somatic and dendritic E_{GABA} and tune SNr responses to Str inputs. (A) Raster plot of spikes in the simulation of an SNr network model containing 50 simulated neurons that receive tonic somatic inhibition from GPe projections. (B) Integrated SNr population activity gives a mean firing rate of about 23 Hz, as seen *in vivo* conditions (***Freeze et al., 2013***; ***Mastro et al., 2017***; ***Willard et al., 2019***). (C) Increasing tonic Cl^- depolarizes somatic and dendritic E_{GABA}. (D) Ramping Str mean firing rate used to represent evidence accumulation in a perceptual decision-making task. (E) Inhibition and pause generation in the SNr during evidence accumulation/ramping Str activity, for two different tonic somatic Cl^- conductance. (F) Increasing the tonic Cl^- conductance lengthens T_{pause}, the time for the SNr firing rate to drop below threshold (colors correspond to threshold levels in E). If the tonic conductance becomes too great, then SNr firing cannot be pushed to arbitrarily low rates.

.

Discussion

In this work, we used computational modeling to explain and make predictions about the responses of SNr neurons to the streams of GABAergic input that they receive from the GPe and striatum (Str), as well as the effects of local interactions within the SNr. Results from previous experiments and from those reported in this paper show that each of these channels, when activated on its own, can induce diverse patterns of SNr spiking. Our simulations show that these responses can result from varying levels of the $GABA_A$ reversal potential, short-term plasticity, and in some cases intracellular Cl^- dynamics. GPe neurons, with somatic synapses on SNr neurons and relatively high sustained firing rates (***Chan et al., 2005***; ***Surmeier et al., 2005***; ***Mastro et al., 2014***; ***Abdi et al., 2015***; ***Deister et al., 2012***), are well positioned to influence E_{GABA} in the SNr and hence to impact SNr processing of GABAergic inputs from other sources. In particular, our results predict that changes in baseline GPe output will modulate the synchrony between SNr neurons coupled through local GABAergic collaterals and can induce or suppress low frequency oscillations in SNr firing. We present data from experiments involving optogenetic stimulation of GPe terminals in SNr supporting this prediction. Moreover, we find that GPe outputs should be able to tune the effectiveness of GABAergic inputs to the SNr from the Str, which may impact the timing of decisions released by pauses in SNr firing.

From a naive perspective, the excitatory and biphasic inhibitory-to-excitatory SNr responses that we observed following stimulation of GPe and Str projections are surprising, since GABAergic synapses are typically considered as inhibitory and the slice preparation used in our experiments largely eliminates the possibility of disinhibitory network effects. Excitatory and biphasic GABAergic effects are not unprecedented, however, as they have been reported in other brain regions (***Haam et al., 2012***; ***Astorga et al., 2015***). Furthermore, from a theoretical perspective, these GABAergic responses are relatively well understood (see (***Dayan and Abbott, 2001***; ***Doyon et al., 2011***, ***2016a***,b)

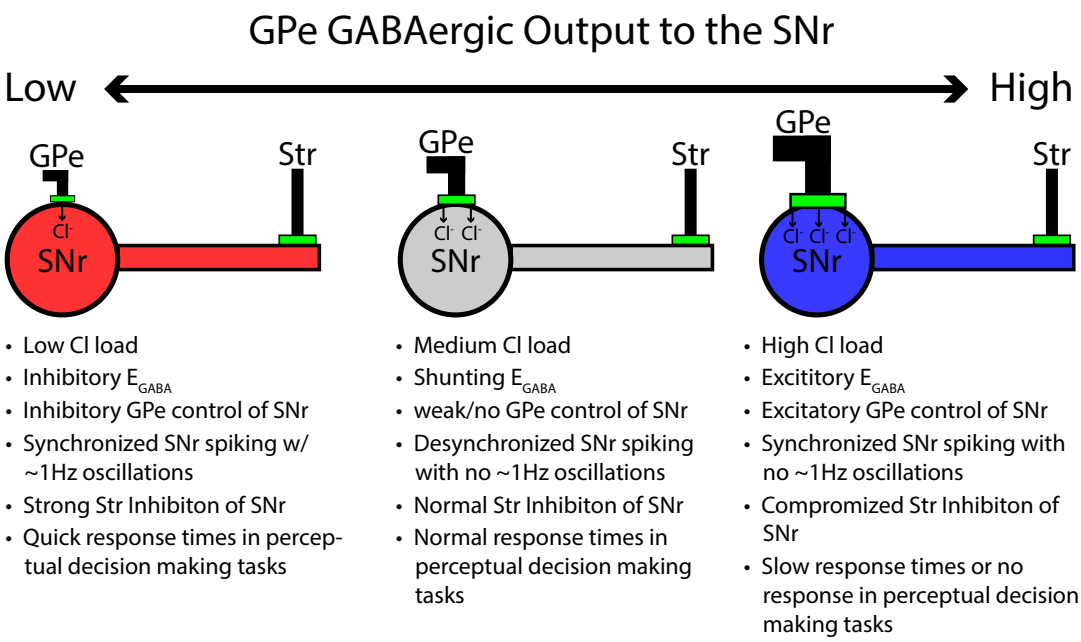

Figure 12. Summary figure/cartoon - GPe output provides tonic Cl load tuning SNr synchrony and the strength of Str inhibition

.

for reviews). The direction (inhibitory versus excitatory) of the GABAergic current (I_{GABA}) depends on the value of E_{GABA} relative to the membrane potential (V_m) when $GABA_A$ receptors are activated. As such, excitatory responses are expected to result from a GABAergic reversal potential (E_{GABA}) that is depolarized close to or above the action potential threshold of a given neuron, while biphasic inhibitory-to-excitatory responses are expected to be mediated by a relatively rapid Cl^- accumulation and ongoing depolarization of E_{GABA} during the arrival of GABAergic inputs, which may be accelerated in small dendritic compartments. In keeping with this idea, stimulation of striatal inputs to SNr in mouse brain slices at a slower rate of 2Hz yielded consistent initial inhibitory effects rather than the diversity of SNr responses we observed (***Simmons et al., 2018***). It is also possible that sustained stimulation of GPe and Str terminals may yield slow short-term depression that contributes to gradual changes in SNr firing rates, but this would not explain the biphasic SNr responses. Similarly, inhibition could recruit additional currents that are activated by hyperpolarization, such as low voltage-activated Ca^{2+}, persistent sodium, or hyperpolarization-activated cyclic nucleotide–gated (HCN) channels, for example. A subset of these currents could theoretically combine to explain the biphasic but not the purely excitatory responses.

As one possible implication of depolarization of E_{GABA}, experiments in rodent epilepsy models have revealed that seizure-like events are preceded by surges in interneuron activity that depolarize E_{GABA}, sparking a positive feedback loop that can result in runaway activity (***Lillis et al., 2012***; ***Kaila et al., 2014***). Interestingly, E_{GABA} has been found to exhibit a strong sensitivity to changes in factors that can affect Cl^- levels (***Kaila et al., 2014***) some of which, such as KCC2-mediated Cl^- extrusion (***Sivakumaran et al., 2015***; ***Moore et al., 2017***; ***Schulte et al., 2018***; ***Titz et al., 2015***), may be tunable by cellular signaling pathways (***Titz et al., 2015***). According to our model, compromised KCC2 function would likely depolarize E_{GABA} , slowing or even preventing decision-making. More generally, our results support the idea that GPe output itself could be modulated to tune SNr processing, related to decision speeds or other functions, in condition-specific ways (see Figure 12).

Our experiments characterizing SNr responses to optogentic stimulation of GPe and Str GABAergic projections were done in *in vitro* slice preparations. In general, the measured value of E_{GABA} is thought to be hyperpolarized in *in vitro* slice preparations relative to *in vivo* conditions (***Doyon***

et al., 2011, *2016a*,b). This difference is predicted to arises due to decreased excitability in slice preparations and severed synaptic projections, which result in an overall reduction of synaptic transmission and, consequently, reduced tonic chloride conductance/load. Applying this idea to the SNr, E_{GABA} should be depolarized in *in vivo* relative to *in vitro* conditions. Values of E_{GABA} measured in the SNr *in vitro* typically range between $-75\,mV$ and $-60\,mV$ (*Connelly et al., 2010*; *Higgs and Wilson, 2016*; *Simmons et al., 2018*) although values as high as $-55\,mV$ have been reported (*Giorgi et al., 2007*) in some conditions. Because spiking in the SNr is asynchronous in control animals (*Deransart et al., 2003*; *Willard et al., 2019*), our model would predict that E_{GABA} should be close to $-55\,mV$ *in vivo* (Fig. 8 A4). If E_{GABA} is depolarized *in vivo* we would also expect to see an increase in the number of SNr neurons that have excitatory responses to optogenetic stimulation of GABAergic projections from GPe neurons of the indirect pathway and Str projections from the direct pathway, relative to our results *in vitro* (Fig. 6). Consistent with this prediction, previous *in vivo* experiments (*Freeze et al., 2013*) found that optogenetic stimulation of D1 Str neurons resulted in excitatory responses in 55% (15 of 27) of SNr neurons.

The impact of GABAergic inputs from GPe on synchrony within SNr predicted by our model is consistent with a previous study that examined the effect of E_{GABA} on dynamics of a bidirectionally coupled neuron pair *Jeong and Gutkin* (*2007*). The previous work also exploited PRCs for its analysis but was done using simpler models, in the context of weak coupling, and did not consider the unidirectional case. In fact, given the sparsity of synaptic collaterals within SNr *Simmons et al.* (*2018*), we expect that unidirectional connectivity between SNr neurons would be the dominant motif observed. Thus, our model suggests that GPe firing rates could tune the level of synchrony in SNr, with oscillations emerging when E_{GABA} is below the afterhyperpolarization potential.

The oscillations that we predict will arise in SNr neurons are slower than the β oscillations often discussed in the context of parkinsonism. These slow oscillations are consistent with previous results in anesthetized animals (*Walters et al., 2007*) and arise in recently reported experiments (*Whalen et al., 2020*) and in the data presented here. Our results, based on the amplitude and shape of PRCs, predict that oscillation frequency will vary with E_{GABA} and with the strength of synapses between SNr neurons (Figure 9) but never reach frequencies in the β band. Various data, simulations and theory suggest different changes in PRC shape with neuronal firing rate (*Tsubo et al., 2007*; *Phoka et al., 2010*; *Couto et al., 2015*; *Ermentrout and Terman, 2010*). Simulations of our model SNr neurons showed a reduction in PRC amplitude with increased presynaptic neuron firing rate, up to saturation around $25\,Hz$, which would lead to the need for more oscillation cycles to occur to achieve one full passage along the PRC (e.g., Fig. 9). This explains why, although more cycles occur in a given time, the slow oscillation frequency does not significantly increase. The mechanism underlying the changes in our model neuron's PRC with input frequency likely depends on the particular currents included but remains for future investigation.

The precise functions of Str inputs to SNr neurons remain unknown. Although there is significant literature supporting a role for these inputs in action selection or initiation, there are certainly other possibilities. One such idea is that Str inputs encode movement velocity and the resulting SNr firing rate encodes spatial position (*Kim et al., 2014*; *Bartholomew et al., 2016*; *Barter et al., 2015*). If we apply our modeling results to this view, then we predict that the Cl^- load from the GPe, by tuning SNr responses to GABAergic inputs from Str, could impact velocity with which selected movements are performed. On the other hand, we do not expect that Str inputs would tune E_{GABA} in SNr and SNr synchrony, as we predict for GPe inputs. This difference arises due to the lower Str baseline firing rate, which would have less impact on Cl^- load, and the dendritic targeting of Str inputs to SNr, which would not induce a strong effect at the soma.

In mice, DA depletion increases SNr synchrony (*Willard et al., 2019*) and promotes slow oscillations (*Whalen et al., 2020*). In our model, this may be explained by a depolarizing shift in E_{GABA} under these conditions, presumably driven by a reduction in GPe firing rate (*Filion et al., 1991*; *Boraud et al., 1998*; *Wichmann et al., 2002*) and/or decreased GABAergic synaptic output to the SNr. Therefore, we would predict GABAergic inhibiton to be stronger in under DA depletion. This

is consistent with previous a previous study which shows that GABAergic inhibition in the SNr is attenuated by activation of D2 receptors (***Martin and Waszczak, 1996***). Additionally, our model predicts that strengthened GABAergic inhibition could enhance the capability of inputs from the Str to pause SNr firing, potentially facilitating action selection. Consistent with this idea, DA depletion has been shown to accelerate saccadic perceptual decisions in humans (***Van Stockum et al., 2011***; ***van Stockum et al., 2013***).

While our model allows for the simulation of multiple sources of GABA to SNr neurons along with somato-dendritic interactions, short-term synaptic plasticity, and time courses of $[Cl^-]$ and E_{GABA} dynamics, it does omit a variety of additional factors that could impact our predictions. Most significantly, to focus on GABAergic effecs, we ignored STN inputs to SNr neurons. In baseline conditions of ongoing high frequency STN activity, these inputs would help tune SNr excitability but we do not expect them to be relevant for adjusting Cl^- load and E_{GABA}; the effects of more patterned STN activity under DA depletion remain to be explored. Secondly, our description of the location of GPe projections on SNr neurons involves some simplification. GPe projections primarily form synapses around the soma but also form synapses on proximal dendrites (***Smith and Bolam, 1991***; ***Von Krosigk et al., 1992***), which we have ignored. The study conducted by ***Smith and Bolam*** (***1991***) found that SNr-projecting GPe neurons formed synapses with the soma and the distal dendrites of 54% and 32% of SNr neurons, respectively. Although our model does not distinguish among the diverse subpopulations of GPe neurons that have been identified (***Mastro et al., 2014***; ***Hernández et al., 2015***; ***Abdi et al., 2015***), an intriguing possibility for future study is that different subsets of GPe neurons may project to different sites on SNr neurons, allowing for separable control over local SNr interactions and synchrony versus responses to Str inputs. Along similar lines, we assumed that GABAergic SNr collaterals form somatic as opposed to dendritic synapses. We also did not model non-neuronal cells such as glia that can affect extracellular ion concentrations, which could reduce the amplitude of the effects that we describe; the variability in extracellular concentrations of ions other than Cl^- such as K^+, which could affect SNr excitability; slower components of synaptic depression that, if present, may yield a gradual weakening of inhibition over several seconds; and direct effects of DA and other neuromodulators.

We have cited and shown that our results are consistent with a range of experimental data. To really pin down the relevance of these ideas, future experiments would need to be performed to measure intracellular $[Cl^-]$ or E_{GABA} itself. For the latter, it may be possible to perform perforated patch recordings and measure E_{GABA} as a function of GPe firing rate, but these experiments are challenging and may not be possible in dendrites. If they are born out by future experiments, the findings of this study may have implications outside of the SNr, as $GABA_A$ is a major neurotransmitter in the CNS.

Methods and Materials

Model description

Model SNr neurons were developed that each feature both a somatic and a dendritic compartment and incorporate Hodgkin-Huxley style conductances adapted from previously described models and/or experimental data (***Xia et al., 1998***; ***Zhou et al., 2008***; ***Corbit et al., 2016***; ***Doyon et al., 2016a***). The membrane potentials for the somatic (V_S) and dendritic compartments (V_D) are given by the following differential equations:

$$C_S \frac{dV_S}{dt} = -I_{Na} - I_{NaP} - I_K - I_{Ca} - I_{SK} - I_{Leak} - I^S_{GABA} - I_{DS} + I_{APP} \tag{1}$$

$$C_D \frac{dV_D}{dt} = -I_{TRPC3} - I^D_{GABA} - I_{SD} \tag{2}$$

where $C_S = 100\,pF$ and $C_D = 20\,pF$ are the capacitances for the somatic and dendritic compartments. The currents in each compartment are represented by I_i where i denotes the current type. The somatic compartment features the essential spike generating currents as well as several others: fast Na^+ current (I_{Na}), persistent Na^+ current (I_{NaP}), delayed rectifying K^+ current (I_K), Ca^{2+} current (I_{Ca}), Ca^{2+}-activated K^+ current (I_{SK}), and leak current (I_{Leak}) as well as a synaptic current which represents the GABAergic input from the GPe neurons of the indirect pathway (I^S_{GABA}). I_{APP} denotes an applied current injected from an electrode. The dendritic compartment contains a current from a transient receptor potential channel 3 (TRPC3) (I_{TRPC3}) and a synaptic current (I^D_{GABA}), which represents the GABAergic input from the striatal neurons of the direct pathway. The two additional currents I_{DS} and I_{SD} are coupling terms that represent the current from the dendrite into the soma and from the soma into the dendrite, respectively. The currents are defined as follows:

$$I_{Na} = g_{Na} \cdot m^3_{Na} \cdot h_{Na} \cdot s_{Na} \cdot (V_S - E_{Na}) \tag{3}$$

$$I_{NaP} = g_{NaP} \cdot m^3_{NaP} \cdot h_{NaP} \cdot (V_S - E_{Na}) \tag{4}$$

$$I_K = g_K \cdot m^4_K \cdot h_K \cdot (V_S - E_K) \tag{5}$$

$$I_{Ca} = g_{Ca} \cdot m_{Ca} \cdot h_{Ca} \cdot (V_S - E_{Ca}) \tag{6}$$

$$I_{SK} = g_{SK} \cdot m_{SK} \cdot (V_S - E_K) \tag{7}$$

$$I_{Leak} = g_{Leak} \cdot (V_S - E_{Leak}) \tag{8}$$

$$I^S_{GABA} = g^S_{GABA} \cdot (V_S - E^S_{GABA}) \tag{9}$$

$$I_{DS} = \frac{g_C}{\alpha_C} \cdot (V_S - V_D) \tag{10}$$

$$I_{TRPC3} = g_{TRPC3} \cdot (V_D - E_{TRPC3}) \tag{11}$$

$$I^D_{GABA} = g^D_{GABA} \cdot (V_D - E^D_{GABA}) \tag{12}$$

$$I_{SD} = \frac{g_C}{1 - \alpha_C} \cdot (V_D - V_S), \tag{13}$$

where g_i is the maximum conductance, E_i is the reversal potential, and m_i and h_i are gating variables

for channel activation and inactivation for each current I_i. s_{Na} is an additional inactivation term governing spike-frequency adaptation. The parameter $\alpha_C = 0.833$ is the ratio of somatic and total capacitances. The GABAergic synaptic conductances g^S_{GABA}, g^D_{GABA} are variable and will be defined below. The values used for the g_i and E_i are given in Table 1.

Table 1. Ionic Channel Parameters.

Channel	Parameters		
I_{Na}	$g_{Na} = 35\,nS/pF$	$E_{Na} = 50.0\,mV$	
	$m_{1/2} = -30.2\,mV$	$k_m = 6.2\,mV$	
	$\tau^0_m = 0.05\,ms$	$\tau^1_m = 0.05\,ms$	$\tau^m_{1/2} = 1\,mV$
	$\sigma^0_m = 1\,mV$	$\sigma^1_m = 1\,mV$	
	$h_{1/2} = -63.3\,mV$	$k_h = -8.1\,mV$	
	$\tau^0_h = 0.59\,ms$	$\tau^1_h = 35.1\,ms$	$\tau^h_{1/2} = -43.0\,mV$
	$\sigma^0_h = 10\,mV$	$\sigma^1_h = -5\,mV$	
	$s_{1/2} = -30.0\,mV$	$k_s = -0.4\,mV$	
	$\tau^0_s = 10\,ms$	$\tau^1_s = 50\,ms$	$\tau^s_{1/2} = -40\,mV$
	$\sigma^0_s = 18.3\,mV$	$\sigma^1_s = -10\,mV$	$s_{min} = 0.15$
I_{NaP}	$g_{NaP} = 0.175\,nS/pF$		
	$m_{1/2} = -50.0\,mV$	$k_m = 3.0\,mV$	
	$\tau^0_m = 0.03\,ms$	$\tau^1_m = 0.146\,ms$	$\tau^m_{1/2} = -42.6\,mV$
	$\sigma^0_m = 14.4\,mV$	$\sigma^1_m = -14.4\,mV$	$m_{min} = 0.0$
	$h_{1/2} = -57.0\,mV$	$h_m = -4.0\,mV$	
	$\tau^0_h = 10.0\,ms$	$\tau^1_h = 17.0\,ms$	$\tau^h_{1/2} = -34.0\,mV$
	$\sigma^0_h = 26.0\,mV$	$\sigma^1_h = -31.9\,mV$	$h_{min} = 0.154$
I_K	$g_K = 50\,nS/pF$	$E_K = -90.0\,mV$	
	$m_{1/2} = -26\,mV$	$k_m = 7.8\,mV$	
	$\tau^0_m = 0.1\,ms$	$\tau^1_m = 14.0\,ms$	$\tau^m_{1/2} = -26.0\,mV$
	$\sigma^0_m = 13.0\,mV$	$\sigma^1_m = -12.0\,mV$	
	$h_{1/2} = -20.0\,mV$	$h_m = -10.0\,mV$	
	$\tau^0_h = 5.0\,ms$	$\tau^1_h = 20.0\,ms$	$\tau^h_{1/2} = 0.0\,mV$
	$\sigma^0_h = 10.0\,mV$	$\sigma^1_h = -10.0\,mV$	$h_{min} = 0.6$
I_{Ca}	$g_{Ca} = 0.7\,nS/pF$	$E_{Ca} = 13.27 \cdot ln(Ca_{out}/Ca_{in})$	
	$Ca_{out} = 4.0\,mM$	Ca_{in}, see Eq. 18	
	$m_{1/2} = -27.5\,mV$	$k_m = 3.0\,mV$	$\tau_m = 0.5\,ms$
	$h_{1/2} = -52.5\,mV$	$k_h = -5.2\,mV$	$\tau_h = 18.0\,ms$
I_{SK}	$k_{SK} = 0.4\,mM$	$n_{SK} = 4$	$\tau_{sk} = 0.1\,mS$
I_{Leak}	$g_{Leak} = 0.04\,nS/pF$	$E_{Leak} = -60\,mV$	
I^S_{GABA}	$W^{GPe}_{GABA} = 0.2\,nS/pF$	E^S_{GABA}, see Eq. 23	$\tau_{SynE} = 3.0\,ms$
	$D_0 = 1.0$	$\alpha_D = 0.565$	$\tau_D = 1000\,ms$
	$D_{min} = 0.67$	$W^{SNr}_{GABA} = 0.1\,nS/pF$	
I_{SD}, I_{DS}	$g_C = 0.65\,nS/pF$		
I_{TRPC3}	$g_{TRPC3} = 0.1\,nS/pF$	$E_{TRPC3} = -37.0\,mV$	
I^D_{GABA}	$W^{Str}_{GABA} = 0.4\,nS/pF$	E^D_{GABA}, see Eq. 23	$\tau^D_{GABA} = 7.2\,ms$
	$F_0 = 0.145$	$\alpha_F = 0.125$	$\tau_F = 1000\,ms$

Activation (m_i) and inactivation (h_i, s_i) of voltage-dependent channels are described as follows:

$$\frac{dz_i}{dt} = \frac{z^\infty_i - z_i}{\tau_{z_i}}, \quad i = \{Na, NaP, K, Ca\}, \quad z = \{m, h, s\}. \tag{14}$$

Steady-state (in)activation functions and their time constants (τ_{z_i}) are described by:

$$z_i^{\infty}(V) = \frac{1}{1 + e^{-(V - z_{1/2}^i)/k_{z_i}}}, \tag{15}$$

$$\tau_{z_i}(V) = \tau_{z_i}^0 + \frac{\tau_{z_i}^1 - \tau_{z_i}^0}{e^{(\tau_{1/2}^i - V)/\sigma_{z_i}^0} + e^{(\tau_{1/2}^i - V)/\sigma_{z_i}^1}}. \tag{16}$$

The parameters for these currents are given in Table 1 and were adapted from ***Corbit et al.*** (***2016***).

Activation of the small conductance calcium-activated potassium channels (SK) is instantaneous and depends on the intracellular calcium concentration ($[Ca]_i$):

$$m_{SK}([Ca]_{in}) = \left(1 + \left(\frac{k_{SK}}{[Ca]_{in}}\right)^{n_{SK}}\right)^{-1}, \tag{17}$$

where k_{SK} represents the half-activation Ca^{2+} concentration and n_{SK} is the Hill coefficient. The parameters are given in Table 1 and were taken from ***Xia et al.*** (***1998***).

The intracellular calcium concentration is determined by the balance of Ca^{2+} influx carried by I_{Ca} and efflux via the Ca^{2+} pump. In the model, I_{Ca} and I_{SK} are only expressed in the soma and therefore $[Ca]_{in}$ dynamics is only simulated in the somatic compartment. Dynamics of $[Ca]_{in}$ are described by the following equation:

$$\frac{d[Ca]_{in}}{dt} = -\alpha_{ca} \cdot I_{Ca} - ([Ca]_{in} - Ca_{min})/\tau_{Ca}, \tag{18}$$

where $\alpha_{ca} = 1.0 \cdot 10^{-8} mM/fC$ is a conversion factor relating current and rate of change in $[Ca]_{in}$, $\tau_{Ca} = 250\,ms$ is the time constant for the Ca^{2+} extrusion and $Ca_{min} = 5.0 \cdot 10^{-8}\,mM$ is the minimum calcium concentration.

Synaptic dynamics

The GABAergic synaptic conductance in the somatic (g_{GABA}^S) and dendritic g_{GABA}^S compartments are described by the following equations:

$$\frac{dg_{GABA}^S}{dt} = -\frac{g_{GABA}^S}{\tau_{GABA}^S} + W_{GABA}^{GPe} \cdot D \cdot \delta(t - t_n) + W_{GABA}^{SNr} \cdot \delta(t - t_m), \tag{19}$$

and

$$\frac{dg_{GABA}^D}{dt} = \frac{g_{GABA}^D}{\tau_{GABA}^D} + W_{GABA}^{Str} \cdot F \cdot \delta(t - t_l), \tag{20}$$

where $\tau_{GABA}^{\{S,D\}}$ is the exponential decay time constant for the somatic and dendritic compartments, $W_{GABA}^{\{GPe,SNr,Str\}}$ is the synaptic weight of inputs from the GPe, SNr, and Str. $\delta(.)$ represents the Kronecker delta function, t is time, and $t_{\{n,m,l\}}$ represent the times that inputs n, m, l are received from GPe, SNr, and Str, respectively. The functions D and F are scaling factors representing short-term synaptic depression and facilitation, which were simulated using an established mean-field model of short-term synaptic depression/facilitation (***Abbott et al., 1997***; ***Dayan and Abbott, 2001***; ***Morrison et al., 2008***) as follows:

$$\frac{dD}{dt} = \frac{D_0 - D}{\tau_D} - \alpha_D(D - D_{min}) \cdot \delta(t - t_i), \tag{21}$$

and

$$\frac{dF}{dt} = \frac{F_0 - F}{\tau_F} + \alpha_F(1 - F) \cdot \delta(t - t_k). \tag{22}$$

The parameters for D_0, τ_D, α_D, D_{min}, F_0, τ_F, and α_F are listed in Table 1 and were chosen to empirically match experimental data from ***Connelly et al.*** (***2010***), see Fig. 2.

Chloride and E_{GABA} Dynamics

GABA$_A$ receptors are permeable to both Cl^- and $HCO3^-$ ions. Therefore, the reversal potential E_{GABA} is a function of ion concentration gradients for both of these substances and is determined by the Goldman–Hodgkin–Katz voltage equation:

$$E_{GABA} = \frac{RT}{F} \cdot ln\left(\frac{4[Cl^-]_{in} + [HCO_3^-]_{in}}{4[Cl^-]_{out} + [HCO_3^-]_{out}}\right), \tag{23}$$

where $R = 8.314\,J/(mol\,K)$ is the universal gas constant; $T = 308\,K$ is temperature; $F = 96.485\,kC/mol$ is the Faraday constant. The concentrations $[Cl^-]_{out} = 120\,mM$ $[HCO_3^-]_{in} = 11.8\,mM$, $[HCO_3^-]_{out} = 25.0\,mM$ are fixed parameters representing the extracellular Cl^- and intracellular and extracellular $HCO3^-$ concentrations, respectively. Parameters were adapted from ***Doyon et al.*** (***2016a***). The intracellular Cl^- concentration in the somatic ($[Cl^-]_{in}^S$) and dendritic ($[Cl^-]_{in}^D$) compartments is dynamic and is determined by the balance of Cl^- influx through GABAergic synapses (I_{GABA}) and efflux via the KCC2 Cl^- extruder. In both compartments, the dynamics of $[Cl]_{in}$ is governed by the following equation:

$$\frac{d[Cl^-]_{in}}{dt} = \alpha_{Cl} \cdot \left[g_{KCC2} \cdot (E_{Cl} - E_k) - \chi \cdot (g_{GABA} + g_{GABA}^{Tonic}) \cdot (V - E_{Cl})\right], \tag{24}$$

$$\chi = \frac{V - E_{CL}}{V - E_{GABA}}, \quad \text{and} \quad E_{Cl} = \frac{RT}{F} \cdot ln\left(\frac{Cl_{out}}{Cl_{in}}\right). \tag{25}$$

In the previous equations, α_{Cl} is a conversion factor relating current and rate of change in $[Cl]_{in}$, g_{KCC2}, g_{GABA} and g_{GABA}^{Tonic} are the conductances of the KCC2 Cl^- extruder, GABAergic conductance, and tonic chloride load. χ describes the fraction of the $GABA_A$ current that is carried by Cl^- ions, and V represents the membrane potential of the specific compartment. The dynamics of Cl^- are simulated separately for the somatic ($[Cl]_{in}^S$) and dendritic ($[Cl]_{in}^D$) compartments, which have distinct α_{Cl} values, specifically $1.77 \cdot 10^{-7}\,mM/fC$ and $2.2125 \cdot 10^{-7}\,mM/fC$ for the somatic and dendritic compartments. In both compartments g_{KCC2} and g_{GABA}^{Tonic} are parameters which are varied to tune E_{GABA}. Specifically, g_{KCC2} is varied from 0.0 to $0.4\,nS/pF$ and g_{GABA}^{Tonic} is from 0.0 to $1.0\,nS/pF$. E_K is fixed and can be found in Table 1. This mathematical description of Cl^- dynamics was adapted from ***Doyon et al.*** (***2016a***).

Phase Response Curves

The dataset for calculating the phase response curves were generated by simulating transient GABAergic inputs to the somatic compartment every $2\,s$ plus a randomly generated variation of 0 to $100\,ms$. The dataset was post-processed in Matlab and for each simulated GABAergic input, the change in phase relative to the input phase was extracted. Equations for the PRCs were generated using a forth order polynomial fit.

Bidirectional network: Phase on the horizontal axis is defined in a frame relative to the phase of neuron 1. In other words, to compute the PRC of neuron 2, we consider the effect of an input from neuron 1 to neuron 2 when neuron 2 is at different phases; the fact that neuron 1 is supplying the input means that the phase of neuron 1 is 1. To compute the PRC of neuron 1, we should still think of the phase of neuron 1 as being 1 (or equivalently 0), but now neuron 2 is the neuron providing the input. As a result, the PRC for neuron 1 ends up being given by reflecting the PRC for neuron 2 about 0.5.

For example, suppose that the phase of neuron 2 is altered by an amount $\Delta\phi$ if it receives an input when it is at phase 0.8, such that the PRC of neuron 2 takes the value $\Delta\phi$ at phase $\phi = 0.8$. Note that at $\phi = 0.8$, neuron 2 lags neuron 1 by a phase of 0.2. Now, at what phase should the PRC for neuron 1 take the value $\Delta\phi$? To answer this question, we must determine the phase of neuron 2 when it spikes, given that neuron 1 lags neuron 2 by 0.2. But since the phase of neuron 1 is 0, we simply conclude that the value $\Delta\phi$ occurs on the PRC of neuron 1 at $\phi = 0.2$ (i.e., at $\phi = 1 - 0.8$).

SNr network construction

As mentioned above, the SNr is a sparsely connected network where each neuron is estimated to receive between 1-4 inputs from neighboring SNr neurons (***Higgs and Wilson, 2016***). To represent sparse connectivity in our simulated 100 neuron SNr network (see Fig. 11 A), equation (19) for g^S_{GABA} was slightly modified such that the somatic GABAergic conductance in the i^{th} neuron in the population is described by the following equation:

$$g^S_{GABA} = \sum_{j \neq i;n} W^{SNr}_{j,i} \cdot C_{ji} \cdot H(t - t_{j,n}) \cdot e^{-(t-t_{j,n})/\tau^S_{GABA}}, \tag{26}$$

where $W^{SNr}_{j,i}$ is the weights of the SNr to SNr synaptic connection from source neuron j to the target neuron i. C_{ji} is a connectivity matrix where $C_{ji} = 1$ if neuron j makes a synapse on neuron i, and $C_{ji} = 0$ otherwise. $H(.)$ is the Heaviside step function, and t denotes time. $t_{j,n}$ is the time at which the n^{th} action potential is generated in neuron j and reaches neuron i. Sparse connectivity in the model was achieved by randomly assigning the vales of C_{ji} such that the probability of any connection between neuron i and j being 1 is equal to the 0.02. Heterogeneity in the network was introduced by uniformly distributing the weights of SNr connections such that $W^{SNr}_{j,i} = U(0, 0.1\,nS/pF)$. Additionally, in order to match *in vivo* data (***Freeze et al., 2013***; ***Mastro et al., 2017***; ***Willard et al., 2019***) the baseline firing rate was increased to $\approx 25\,Hz$ by setting $g^D_{Glut} = U(0.020.12)\,nS$. Additionally, diffusion of Cl^- between the somatic and dendritic compartments is incorporated into the network model. This was simulated by the addition of the exponential decay terms $-([Cl]^S_{in} - [Cl]^D_{in})/(\tau_{SD})$ and $-([Cl]^S_{in} - [Cl]^S_{in})/(\tau_{DS})$ into Eq. (24) for the somatic and dendritic compartments respectively. The parameters $\tau_{SD} = 200\,ms$ and $\tau_{DS} = 80\,ms$ are exponential decay time constants.

Data analysis and definitions

Data generated from simulations was post-processed in Matlab (Mathworks, Inc.). An action potential was defined to have occurred in a neuron when its membrane potential V_m increased through $-35mV$. For characterization of the paired pule ratios of simulated GPe and Str inputs (Fig. 2 & 3), the IPSC/IPSP amplitude is defined as the absolute value of the difference between current/potential immediately before the start of the synaptic input and the local maximum occurring in a $10\,ms$ window following the synaptic input. Histograms of population activity were calculated as the number of action potentials per $20\,ms$ bin per neuron with units of $APs/(s \cdot neuron)$.

The response of SNr neurons to optogenetic stimulation of GPe and Str terminals were categorized by breaking up the full $10\,s$ stimulation period into bins. The first $1\,s$ was broken up into $1/3\,s$ bins. The rest of the period was broken into $1\,s$ bins. The spiking in each bin was then compared to baseline using t-tests where a p-value less than 0.05 was considered statistically significant. Each response category was defined as follows: (1) Complete Inhibition: less than two spikes in the full $10\,s$ period, (2) Partial Inhibition: at least one bin is statistically less than baseline and no bins are excited, (3) No Effect: no bins are statistically different than baseline, (4) Excitation: at lease one bin is statistically above baseline and no bins are less than baseline, (5) Biphasic: at lease one bin is statistically below and one above baseline. In order to identify pauses that are longer than can be accounted for by short-term synaptic dynamics, the "long pause" was defined as any pause in spiking that continues after 10 stimulus pulses (steady state is reached after roughly 5 pulses), which equates to $1000\,ms$, $500,ms$, $250\,ms$ and $125\,ms$ for stimulation at $10\,Hz$, $20\,Hz$, $40\,Hz$ and $60\,Hz$, respectively.

Integration methods

All simulations were performed locally on an 8-core Linux-based operating system. Simulation software was custom written in C++. Numerical integration was performed using the first-order Euler method with a fixed step-size (Δt) of $0.025ms$.

Slice electrophysiology

Coronal slices containing SNr (300 µm) were prepared using a VT1000S vibratome (Leica Microsystems) from brains of 6-9-week-old (both male and female) mice that had received ChR2 viral injections 2-4 weeks prior. Slices were cut in carbogenated HEPES ACSF containing the following (in mM): 20 HEPES, 92 NaCl, 1.2 $NaHCO_3$, 2.5 KCl, 1 $MgSO_4$, 2 $CaCl_2$, 30 NaH_2PO_4, 25 glucose, pH 7.25. Slices were allowed to recover for 15 min at 33°C in a chamber filled with N-methyl-D-glucamine-HEPES recovery solution (in mM): 93 N-methyl-D-glucamine, 2.5 KCl, 1.2 NaH_2PO_4, 30 $NaHCO_3$, 20 HEPES, 25 glucose, 10 $MgSO_4$, 0.5 $CaCl_2$. Slices were then held at room temperature for at least 1 h before recording carbogenated HEPES ACSF. Recordings were conducted at 33°C in carbogenated ACSF (in mM) as follows: 125 NaCl, 26 $NaHCO_3$, 1.25 NaH_2PO_4, 2.5 KCl, 12.5 glucose, 1 $MgSO_4$, and 2 $CaCl_2$. Data were collected with a MultiClamp 700B amplifier (Molecular Devices) and ITC-18 analog-to-digital board (HEKA) using Igor Pro software (Wavemetrics, RRID:SCR_000325) and custom acquisition routines (Recording Artist; Richard C. Gerkin, Phoenix). Data were collected at 10 kHz and digitized at 40 kHz. Electrodes were made from borosilicate glass (pipette resistance, 2–6 M). The pipet solution consisted of (in mM): 130 $KMeSO_3$, 10 NaCl, 2 $MgCl_2$, 0.16 $CaCl_2$, 0.5 EGTA, 10 HEPES, 2 Mg-ATP, and 0.3 NaGTP.

Surgery and viral injections

Stereotaxic surgeries for viral transfection of ChR2 (AAV2-hsyn-ChR2-eYFP or AAV2-hsyn-ChR2-mCherry, University of North Carolina Vector Core Facility, virus titer 3.1 × 1012) were performed under isoflurane anesthesia (2%). Burr holes were drilled over the target location (GPe or striatum), and virus was injected using either a Nanoject (Drummond Scientific) and glass pulled pipette or a syringe pump (Harvard Scientific) fitted with a syringe (Hamilton) connected to PE10 tubing and a 30 gauge cannula. Viral injections were performed at p35-p50 and allowed to incubate for 2-4 weeks for optogenetic slice electrophysiology.

Oscillation detection

Oscillating units units were detected by a two-step process as described in ***Whalen et al.*** (***2020***). First, we identified peaks in the $0.5 - 4\ Hz$ range of the power spectrum (computed with Welch's method and corrected for the unit's ISI distribution) and determined if any fell above a confidence interval estimated from high frequency ($100 - 500\ Hz$) power, correcting for multiple comparisons (Bonferroni correction). Then, to distinguish oscillations from 1/f noise, we determined if the mean phase shift at this identified frequency fell below a confidence interval estimated from high frequency phase shift. A unit which passed both these criteria was considered to be oscillating.

Acknowledgments

This study was partially supported by NIH awards R01NS101016, R01NS104835, and R21NS095103 (AG) and NSF awards DMS 1516288 (AG, JR), 1612913 (JR), and 1724240 (JR). Some of the data incorporated into Figure 10 was recorded in the Gittis lab by Kevin Mastro. We thank Tim Whalen for help processing the data for Figure 10, for discussions, and for comments on the manuscript.

Supplementary Material

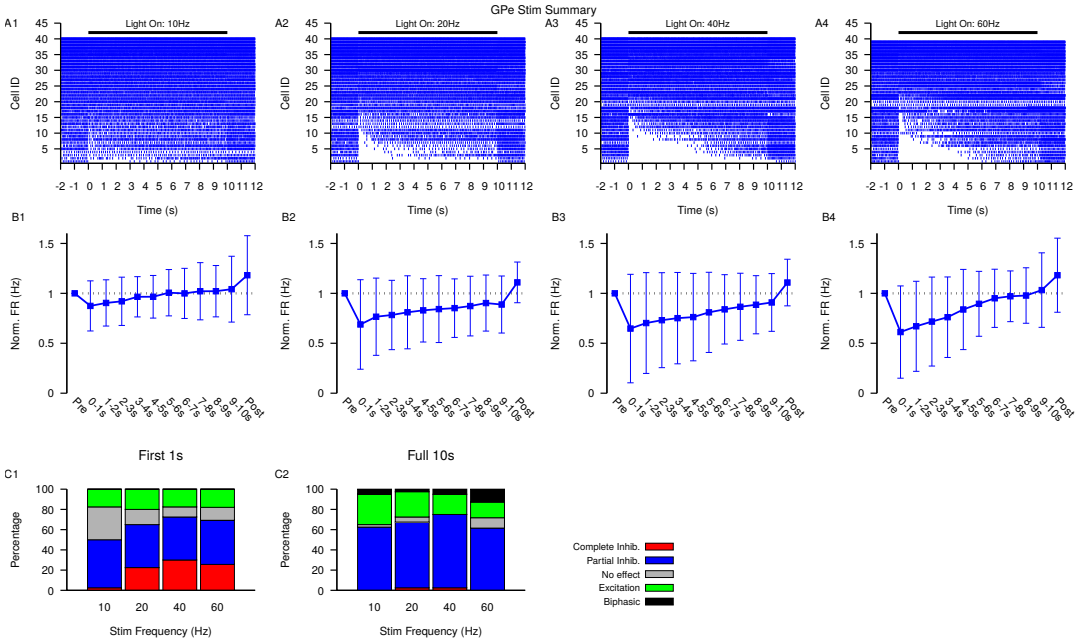

Figure S1. Summary of SNr responses to optogenetic stimulation of GPe synaptic terminals. (A1-A4) Raster plots of spiking sorted by the duration of the pause in spiking at the start of the stimulation period for all SNr neurons tested. (B1-B4) Effect of GPe stimulation on the firing rate of SNr neurons averaged across all neurons and each stimulation frequencies tested. Error bars indicate SD. (C1 & C2) Quantification of types of SNr responses to optogenetic stimulation for varying frequency characterized in the first (C1) $1\,s$ or the full (C2) $10\,s$. Notice that fewer neurons are completely inhibited in the full $10\,s$ period and some biphasic responses emerge.

.

References

Abbott LF, Varela J, Sen K, Nelson S. Synaptic depression and cortical gain control. Science. 1997; 275(5297):221–224.

Abdi A, Mallet N, Mohamed FY, Sharott A, Dodson PD, Nakamura KC, Suri S, Avery SV, Larvin JT, Garas FN, et al. Prototypic and arkypallidal neurons in the dopamine-intact external globus pallidus. Journal of Neuroscience. 2015; 35(17):6667–6688.

Astorga G, Bao J, Marty A, Augustine GJ, Franconville R, Jalil A, Bradley J, Llano I. An excitatory GABA loop operating in vivo. Frontiers in cellular neuroscience. 2015; 9:275.

Atherton JF, Bevan MD. Ionic mechanisms underlying autonomous action potential generation in the somata and dendrites of GABAergic substantia nigra pars reticulata neurons in vitro. Journal of Neuroscience. 2005; 25(36):8272–8281.

Barter JW, Li S, Sukharnikova T, Rossi MA, Bartholomew RA, Yin HH. Basal ganglia outputs map instantaneous position coordinates during behavior. Journal of Neuroscience. 2015; 35(6):2703–2716.

Bartholomew RA, Li H, Gaidis EJ, Stackmann M, Shoemaker CT, Rossi MA, Yin HH. Striatonigral control of movement velocity in mice. European Journal of Neuroscience. 2016; 43(8):1097–1110.

Basso MA, Pokorny JJ, Liu P. Activity of substantia nigra pars reticulata neurons during smooth pursuit eye movements in monkeys. European Journal of Neuroscience. 2005; 22(2):448–464.

Basso MA, Wurtz RH. Neuronal activity in substantia nigra pars reticulata during target selection. Journal of Neuroscience. 2002; 22(5):1883–1894.

Boraud T, Bezard E, Guehl D, Bioulac B, Gross C. Effects of L-DOPA on neuronal activity of the globus pallidus externalis (GPe) and globus pallidus internalis (GPi) in the MPTP-treated monkey. Brain research. 1998; 787(1):157–160.

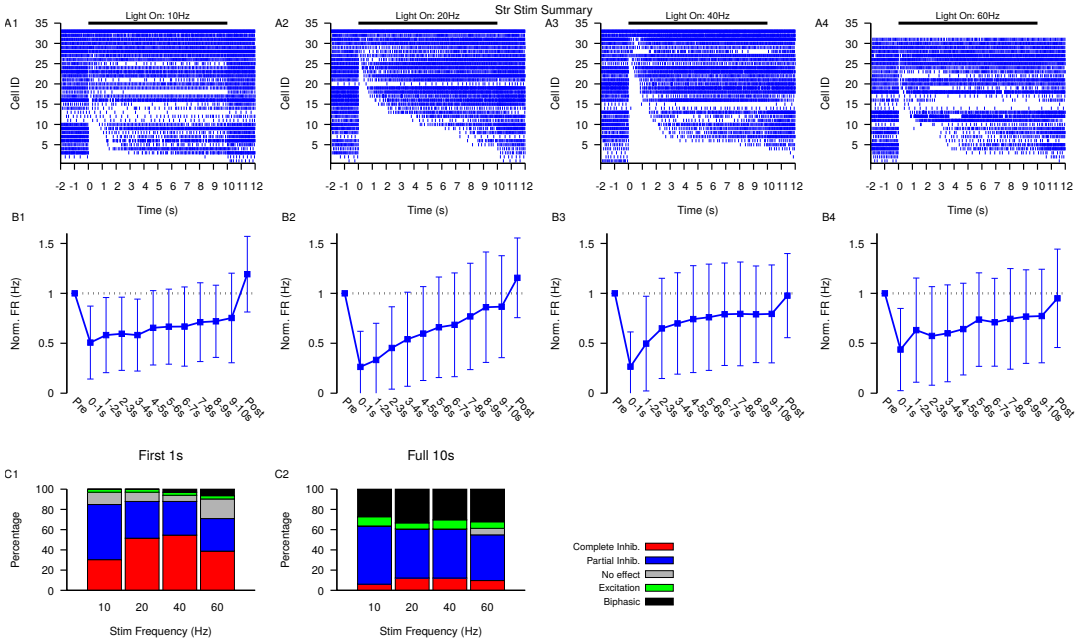

Figure S2. Summary of SNr responses to optogenetic stimulation of Str synaptic terminals. (A1-A4) Raster plots of spiking sorted by the duration of the pause in spiking at the start of the stimulation period for all SNr neurons tested. (B1-B4) Effect of Str stimulation on the firing rate of SNr neurons averaged across all neurons and each stimulation frequencies tested. Error bars indicate SD. (C1 & C2) Quantification of types of SNr responses to optogenetic stimulation for varying frequency characterized in the first (C1) $1\,s$ or the full (C2) $10\,s$. Notice the decrease in the number of completely inhibited neurons and increase in the number of biphasic responses in the full $10\,s$ period.

.

Brown J, Pan WX, Dudman JT. The inhibitory microcircuit of the substantia nigra provides feedback gain control of the basal ganglia output. Elife. 2014; 3:e02397.

Chan CS, Surmeier DJ, Yung WH. Striatal information signaling and integration in globus pallidus: timing matters. Neurosignals. 2005; 14(6):281–289.

Connelly WM, Schulz JM, Lees G, Reynolds JN. Differential short-term plasticity at convergent inhibitory synapses to the substantia nigra pars reticulata. Journal of Neuroscience. 2010; 30(44):14854–14861.

Corbit VL, Whalen TC, Zitelli KT, Crilly SY, Rubin JE, Gittis AH. Pallidostriatal projections promote β oscillations in a dopamine-depleted biophysical network model. Journal of Neuroscience. 2016; 36(20):5556–5571.

Couto J, Linaro D, De Schutter E, Giugliano M. On the firing rate dependency of the phase response curve of rat purkinje neurons in vitro. PLoS computational biology. 2015; 11(3):e1004112.

Dayan P, Abbott LF. Theoretical neuroscience: computational and mathematical modeling of neural systems. . 2001; .

Deister CA, Dodla R, Barraza D, Kita H, Wilson CJ. Firing rate and pattern heterogeneity in the globus pallidus arise from a single neuronal population. Journal of neurophysiology. 2012; 109(2):497–506.

Deransart C, Hellwig B, Heupel-Reuter M, Léger JF, Heck D, Lücking CH. Single-unit analysis of substantia nigra pars reticulata neurons in freely behaving rats with genetic absence epilepsy. Epilepsia. 2003; 44(12):1513–1520.

Ding L, Gold JI. Caudate encodes multiple computations for perceptual decisions. Journal of Neuroscience. 2010; 30(47):15747–15759.

Doyon N, Prescott SA, Castonguay A, Godin AG, Kröger H, De Koninck Y. Efficacy of synaptic inhibition depends on multiple, dynamically interacting mechanisms implicated in chloride homeostasis. PLoS computational biology. 2011; 7(9):e1002149.

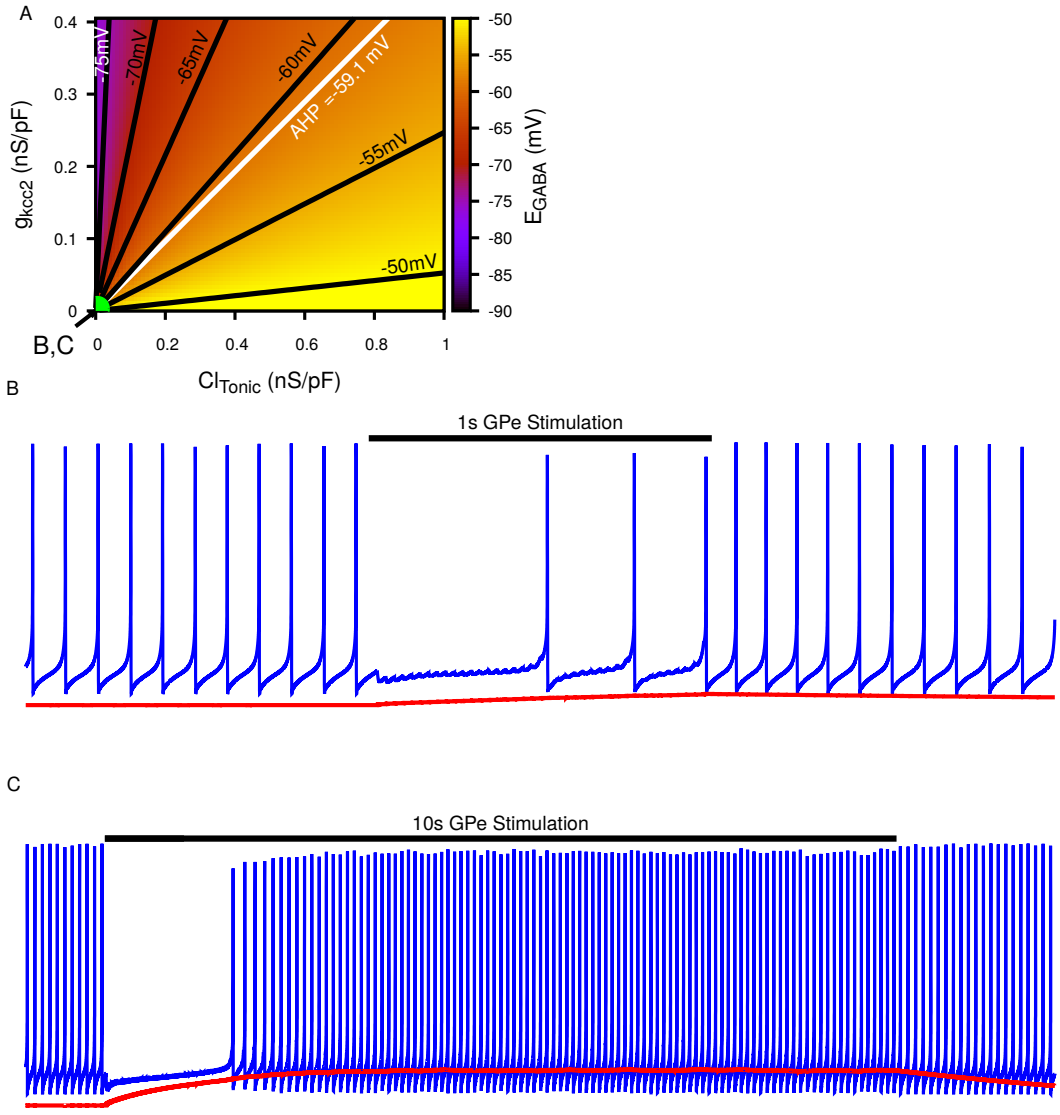

Figure S3. Biphasic SNr response to longer simulated GPe stimulation. (A) Dependence of somatic E_{GABA} on the tonic chloride conductance (g_{GABA}^{Tonic}) and the potassium-chloride co-transporter KCC2 extrusion capacity (g_{KCC2}) as previously shown in Fig. 4 A. (B) Example of "Partial Inhibition" in response to $1\,s$ of stimulation resulting due to a small accumulation of intracellular Cl^-, as shown in Fig. 4 E2. (C) Example of longer $10\,s$ stimulation resulting in larger Cl^- accumulation resulting in a transition of E_{GABA} from inhibitory to excitatory and thus causing a biphasic response in a simulated SNr neuron's firing rate, as seen in $10\,s$ stimulation experiments. g_{GABA}^{Tonic} and g_{KCC2} are the same in (B) and (C) and take the values indicated in (A). To generate the biphasic example the synaptic conductance g_{GABA}^{S} was increased from 0.2 to $0.4\,nS/pF$.

730 **Doyon N**, Prescott SA, De Koninck Y. Mild KCC2 hypofunction causes inconspicuous chloride dysregulation that
731 degrades neural coding. Frontiers in cellular neuroscience. 2016; 9:516.

732 **Doyon N**, Vinay L, Prescott SA, De Koninck Y. Chloride regulation: a dynamic equilibrium crucial for synaptic
733 inhibition. Neuron. 2016; 89(6):1157–1172.

734 **Dunovan K**, Vich C, Clapp M, Verstynen T, Rubin J. Reward-driven changes in striatal pathway competition shape
735 evidence evaluation in decision-making. PLoS computational biology. 2019; 15(5):e1006998.

Ermentrout B. Type I membranes, phase resetting curves, and synchrony. Neural computation. 1996; 8(5):979–1001.

Ermentrout GB, Terman DH. Mathematical foundations of neuroscience, vol. 35. Springer Science & Business Media; 2010.

Filion M, et al. Abnormal spontaneous activity of globus pallidus neurons in monkeys with MPTP-induced parkinsonism. Brain research. 1991; 547(1):140–144.

Freeze BS, Kravitz AV, Hammack N, Berke JD, Kreitzer AC. Control of basal ganglia output by direct and indirect pathway projection neurons. Journal of Neuroscience. 2013; 33(47):18531–18539.

Giorgi FS, Velíšková J, Chudomel O, Kyrozis A, Moshé SL. The role of substantia nigra pars reticulata in modulating clonic seizures is determined by testosterone levels during the immediate postnatal period. Neurobiology of Disease. 2007; 25(1):73–79.

Haam J, Popescu IR, Morton LA, Halmos KC, Teruyama R, Ueta Y, Tasker JG. GABA is excitatory in adult vasopressinergic neuroendocrine cells. Journal of Neuroscience. 2012; 32(2):572–582.

Hernández VM, Hegeman DJ, Cui Q, Kelver DA, Fiske MP, Glajch KE, Pitt JE, Huang TY, Justice NJ, Chan CS. Parvalbumin+ neurons and Npas1+ neurons are distinct neuron classes in the mouse external globus pallidus. Journal of Neuroscience. 2015; 35(34):11830–11847.

Higgs MH, Wilson CJ. Unitary synaptic connections among substantia nigra pars reticulata neurons. Journal of neurophysiology. 2016; 115(6):2814–2829.

Jeong HY, Gutkin B. Synchrony of neuronal oscillations controlled by GABAergic reversal potentials. Neural Computation. 2007; 19(3):706–729.

Kaila K, Pasternack M, Saarikoski J, Voipio J. Influence of GABA-gated bicarbonate conductance on potential, current and intracellular chloride in crayfish muscle fibres. The Journal of Physiology. 1989; 416(1):161–181.

Kaila K, Voipio J. Postsynaptic fall in intracellular pH induced by GABA-activated bicarbonate conductance. Nature. 1987; 330(6144):163.

Kaila K, Ruusuvuori E, Seja P, Voipio J, Puskarjov M. GABA actions and ionic plasticity in epilepsy. Current opinion in neurobiology. 2014; 26:34–41.

Kim N, Barter JW, Sukharnikova T, Yin HH. Striatal firing rate reflects head movement velocity. European Journal of Neuroscience. 2014; 40(10):3481–3490.

Lavian H, Korngreen A. Inhibitory short-term plasticity modulates neuronal activity in the rat entopeduncular nucleus in vitro. European Journal of Neuroscience. 2016; 43(7):870–884.

Lillis KP, Kramer MA, Mertz J, Staley KJ, White JA. Pyramidal cells accumulate chloride at seizure onset. Neurobiology of disease. 2012; 47(3):358–366.

Mahadevan V, Woodin MA. Regulation of neuronal chloride homeostasis by neuromodulators. The Journal of physiology. 2016; 594(10):2593–2605.

Mailly P, Charpier S, Menetrey A, Deniau JM. Three-dimensional organization of the recurrent axon collateral network of the substantia nigra pars reticulata neurons in the rat. Journal of Neuroscience. 2003; 23(12):5247–5257.

Martin LP, Waszczak BL. Dopamine D2 receptor-mediated modulation of the GABAergic inhibition of substantia nigra pars reticulata neurons. Brain research. 1996; 729(2):156–169.

Mastro KJ, Bouchard RS, Holt HA, Gittis AH. Transgenic mouse lines subdivide external segment of the globus pallidus (GPe) neurons and reveal distinct GPe output pathways. Journal of Neuroscience. 2014; 34(6):2087–2099.

Mastro KJ, Zitelli KT, Willard AM, Leblanc KH, Kravitz AV, Gittis AH. Cell-specific pallidal intervention induces long-lasting motor recovery in dopamine-depleted mice. Nature neuroscience. 2017; 20(6):815.

Moore YE, Kelley MR, Brandon NJ, Deeb TZ, Moss SJ. Seizing control of KCC2: a new therapeutic target for epilepsy. Trends in neurosciences. 2017; 40(9):555–571.

Morrison A, Diesmann M, Gerstner W. Phenomenological models of synaptic plasticity based on spike timing. Biological cybernetics. 2008; 98(6):459–478.

Phoka E, Cuntz H, Roth A, Häusser M. A new approach for determining phase response curves reveals that Purkinje cells can act as perfect integrators. PLoS computational biology. 2010; 6(4):e1000768.

Raimondo JV, Markram H, Akerman CJ. Short-term ionic plasticity at GABAergic synapses. Frontiers in synaptic neuroscience. 2012; 4:5.

Ratté S, Prescott SA. ClC-2 channels regulate neuronal excitability, not intracellular chloride levels. Journal of Neuroscience. 2011; 31(44):15838–15843.

Richards C, Shiroyama T, Kitai S. Electrophysiological and immunocytochemical characterization of GABA and dopamine neurons in the substantia nigra of the rat. Neuroscience. 1997; 80(2):545–557.

Sato M, Hikosaka O. Role of primate substantia nigra pars reticulata in reward-oriented saccadic eye movement. Journal of Neuroscience. 2002; 22(6):2363–2373.

Schulte JT, Wierenga CJ, Bruining H. Chloride transporters and GABA polarity in developmental, neurological and psychiatric conditions. Neuroscience & Biobehavioral Reviews. 2018; 90:260–271.

Shires J, Joshi S, Basso MA. Shedding new light on the role of the basal ganglia-superior colliculus pathway in eye movements. Current opinion in neurobiology. 2010; 20(6):717–725.

Simmons D, Higgs MH, Lebby S, Wilson CJ. Predicting responses to inhibitory synaptic input in substantia nigra pars reticulata neurons. Journal of neurophysiology. 2018; 120(5):2679–2693.

Sivakumaran S, Cardarelli RA, Maguire J, Kelley MR, Silayeva L, Morrow DH, Mukherjee J, Moore YE, Mather RJ, Duggan ME, et al. Selective inhibition of KCC2 leads to hyperexcitability and epileptiform discharges in hippocampal slices and in vivo. Journal of Neuroscience. 2015; 35(21):8291–8296.

Smeal RM, Ermentrout GB, White JA. Phase-response curves and synchronized neural networks. Philosophical Transactions of the Royal Society B: Biological Sciences. 2010; 365(1551):2407–2422.

Smith Y, Bolam J. Convergence of synaptic inputs from the striatum and the globus pallidus onto identified nigrocollicular cells in the rat: a double anterograde labelling study. Neuroscience. 1991; 44(1):45–73.

Staley KJ, Proctor WR. Modulation of mammalian dendritic GABAA receptor function by the kinetics of Cl- and HCO3- transport. The Journal of physiology. 1999; 519(3):693–712.

Staley KJ, Soldo BL, Proctor WR. Ionic mechanisms of neuronal excitation by inhibitory GABAA receptors. Science. 1995; 269(5226):977–981.

van Stockum S, MacAskill MR, Myall D, Anderson TJ. A perceptual discrimination task results in greater facilitation of voluntary saccades in Parkinson's disease patients. European Journal of Neuroscience. 2013; 37(1):163–172.

Surmeier DJ, Mercer JN, Chan CS. Autonomous pacemakers in the basal ganglia: who needs excitatory synapses anyway? Current opinion in neurobiology. 2005; 15(3):312–318.

Thounaojam US, Cui J, Norman SE, Butera RJ, Canavier CC. Slow noise in the period of a biological oscillator underlies gradual trends and abrupt transitions in phasic relationships in hybrid neural networks. PLoS computational biology. 2014; 10(5):e1003622.

Titz S, Sammler EM, Hormuzdi SG. Could tuning of the inhibitory tone involve graded changes in neuronal chloride transport? Neuropharmacology. 2015; 95:321–331.

Tsubo Y, Takada M, Reyes AD, Fukai T. Layer and frequency dependencies of phase response properties of pyramidal neurons in rat motor cortex. European Journal of Neuroscience. 2007; 25(11):3429–3441.

Van Stockum S, MacAskill MR, Myall D, Anderson TJ. A perceptual discrimination task abnormally facilitates reflexive saccades in Parkinson's disease. European Journal of Neuroscience. 2011; 33(11):2091–2100.

Von Krosigk M, Smith Y, Bolam J, Smith A. Synaptic organization of GABAergic inputs from the striatum and the globus pallidus onto neurons in the substantia nigra and retrorubral field which project to the medullary reticular formation. Neuroscience. 1992; 50(3):531–549.

828 **Walters JR**, Hu D, Itoga CA, Parr-Brownlie LC, Bergstrom DA. Phase relationships support a role for coordinated
829 activity in the indirect pathway in organizing slow oscillations in basal ganglia output after loss of dopamine.
830 Neuroscience. 2007; 144(2):762–776.

831 **Wei W**, Rubin JE, Wang XJ. Role of the indirect pathway of the basal ganglia in perceptual decision making.
832 Journal of Neuroscience. 2015; 35(9):4052–4064.

833 **Whalen T**, Willard A, Rubin J, Gittis A, Delta Oscillations Are a Robust Biomarker of Dopamine Depletion Severity
834 and Motor Dysfunction in Awake Mice; 2020. In review.

835 **Wichmann T**, Kliem MA, Soares J. Slow oscillatory discharge in the primate basal ganglia. Journal of neurophysi-
836 ology. 2002; 87(2):1145–1148.

837 **Willard AM**, Isett BR, Whalen TC, Mastro KJ, Ki CS, Mao X, Gittis AH. State transitions in the substantia nigra
838 reticulata predict the onset of motor deficits in models of progressive dopamine depletion in mice. eLife.
839 2019; 8:e42746.

840 **Xia XM**, Fakler B, Rivard A, Wayman G, Johnson-Pais T, Keen J, Ishii T, Hirschberg B, Bond C, Lutsenko S, et al.
841 Mechanism of calcium gating in small-conductance calcium-activated potassium channels. Nature. 1998;
842 395(6701):503.

843 **Yanovsky Y**, Velte S, Misgeld U. Ca2+ release-dependent hyperpolarizations modulate the firing pattern of
844 juvenile GABA neurons in mouse substantia nigra pars reticulata in vitro. The Journal of physiology. 2006;
845 577(3):879–890.

846 **Zhou FW**, Matta SG, Zhou FM. Constitutively active TRPC3 channels regulate basal ganglia output neurons.
847 Journal of Neuroscience. 2008; 28(2):473–482.